Computational Nanostructure Design for Hydrogen Storage

Jianjun Liu, James Tyrrell and Qingfeng Ge

Abstract Developing an efficient and affordable hydrogen-storage technology for on-board vehicular applications is a grand challenge to the success of a hydrogen economy. This challenge provides great opportunities for nanoscience and nano-engineering. Novel synthesis and characterization methods allow for an unprecedented degree of manipulation and tracking of the atomic structure in nanoassemblies. Furthermore, computational tools based on density functional theory, which combine fundamental predictive power with atomic resolution, provide a complementary and powerful means for the study and characterization of existing materials and prediction of new compounds and structural motifs, including those for hydrogen storage. In this chapter, we review the development of density functional theory-based computational studies of nanostructure design for hydrogen storage. Our emphasis is on complex metal hydrides. We also discuss the new developments in high surface area materials, including carbon-based materials, and metal- and covalent organic framework-based materials.

1 Introduction and Scope

In his lecture entitled "Our Energy Challenge" given at Southern Illinois University on April 3, 2005, the late Professor Richard E. Smalley identified "Energy" as No.1 on his list of Humanity's top ten problems for the next 50 years. Fossil fuels in the form of coal, oil, and natural gas have been the main source of energy since the industrial revolution. World energy consumption has been

J. Liu · J. Tyrrell · Q. Ge (✉)
Department of Chemistry and Biochemistry, Southern Illinois University, Carbondale, IL 62901, USA
e-mail: qge@chem.siu.edu

L. Zang (ed.), *Energy Efficiency and Renewable Energy Through Nanotechnology*, Green Energy and Technology, DOI: 10.1007/978-0-85729-638-2_22,

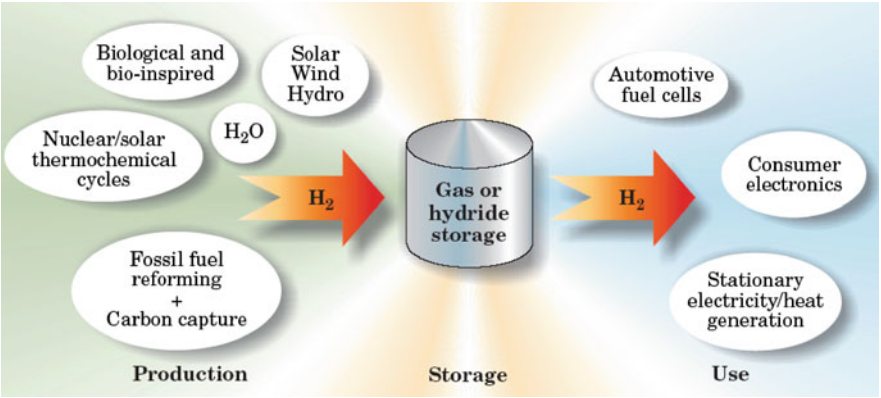

Fig. 1 The hydrogen economy as a network of primary energy sources linked to multiple end users through hydrogen as an energy carrier. Reprinted with permission from [3]. Copyright 2004, American Institute of Physics

constantly increasing since then. However, the supply of fossil fuel is limited. Furthermore, the use of fossil fuel puts human health at risk through chemical and particulate pollutants and affects the global climate through CO_2 and other greenhouse gas emissions. Professor Smalley suggested that *nanotechnology* "holds the answer to most of our pressing material needs", including hydrogen storage, a view shared by many scientists and engineers [1].

Hydrogen is a promising alternative to fossil fuel as an energy carrier. Similar to electricity, hydrogen needs to be produced using a different energy source, such as solar or nuclear. Once hydrogen is produced, a hydrogen-based energy system with a competitive fuel cell technology only produces water and, therefore, is pollution-free [2]. Crabtree et al. described the hydrogen economy as a network composed of three functional steps: production, storage, and use, as depicted in Fig. 1 [3]. These authors indicated that storing hydrogen in a high-energy–density form is a key element of the hydrogen economy, especially for on-board vehicular applications.

For on-board applications, the hydrogen storage systems are required to provide the needed quantity of hydrogen with acceptable volume, weight, cost, and safety risk compared to the current gasoline-driven combustion engine [4]. The available hydrogen storage modalities – including compressed gaseous hydrogen, cryogenic liquid hydrogen, and metal hydrides – each meet some, but not all, of the requirements for critical applications, as shown in Fig. 2 [5]. Therefore, developing a compact and efficient hydrogen-storage technology is the most technically challenging aspect of achieving a hydrogen economy.

Solid-state hydrogen storage, using nanoscience and nanotechnology, offers perhaps the best opportunity for meeting the requirements of on-board applications. Nanoscience and nanotechnology involve studying and working with matter on a nanometer scale. Nanomaterials are categorized as those that have structural components with at least one dimension smaller than 100 nm. Nanomaterials can

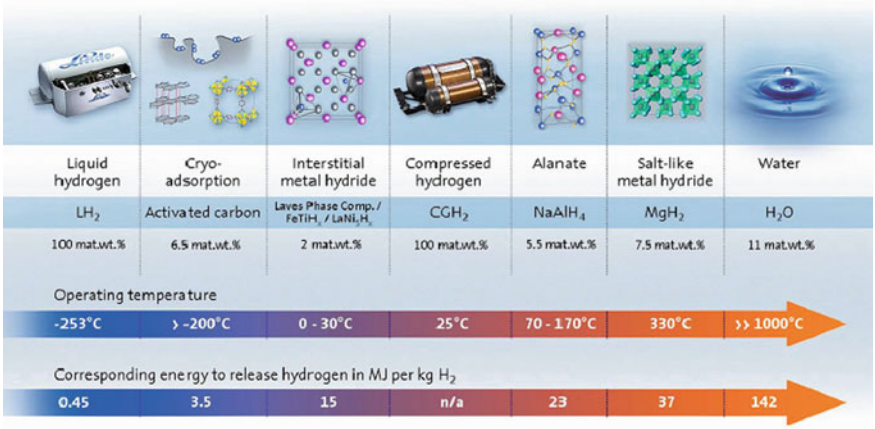

Fig. 2 Available hydrogen-storage technology and the corresponding operating conditions. Reprinted from [5], Copyright 2007, with permission from Elsevier

be in the form of thin films or surface coatings, nanowires and nanotubes, or nanoparticles. The unique properties of nanomaterials originate from the increased surface area and quantum effects, both of which relate to the small size. Consequently, the reactivity, strength and electrical characteristics of nanomaterials may be significantly different from those of conventional materials. For example, a particle of size 30 nm has only 5% of its atoms on its surface. When the size is reduced to 3 nm, the particle has 50% of its atoms exposed on the surface. This gives nanoparticles a much greater surface area per unit mass than larger particles. Both surface area and exposed atoms on the surface could be useful for storing hydrogen. Therefore, nanotechnology is expected to play a key role, as suggested by Smalley, in designing high-capacity solid-state hydrogen storage materials. In fact, the concept of nanoscience and nanoengineering has been actively exploited in improving existing hydrogen storage materials and searching for new hydrogen storage candidates. For example, nanocatalysts have been used to improve the kinetics of hydrogen uptake and release [6] and to improve hydrogen storage capacity through spillover [7]. Novel building blocks have been proposed to maximize the hydrogen capacity and optimize the strength of hydrogen binding [8]. Large-surface area nanomaterials that offer more host atoms/sites for hydrogen and allow easy access to these sites have been synthesized in materials such as metal-organic frameworks (MOFs) [9] and covalent organic frameworks (COFs) [10], and show promise as hydrogen storage media.

Depending on the nature of the hydrogen interaction with the storage media, solid-state hydrogen storage materials can be categorized into two groups: atomically bound hydrogen in either hydrides or other compounds (amines or imides) and molecularly adsorbed hydrogen in highly porous materials. The two groups can also be combined, e.g., using the high surface area material as a support/scaffold for hydrides or other hydrogen-containing compounds.

For all hydrogen storage materials, structural information is critical to understand their properties and performance. However, experimentally determining the structure of materials at the nanometer scale, especially for those materials involving hydrogen, is extremely challenging. Tracking the chemistry of hydrogen is even more difficult. On the other hand, computational chemistry and molecular simulation are advantageous for studies of well-defined systems, including those containing hydrogen. First-principles approaches developed on the basis of density functional theory (DFT) [11, 12] and implemented for both clusters and periodic slabs can handle systems significantly larger than those using traditional ab initio methods. The combined predictive power and atomic resolution provide a quantitative characterization of new materials. They have been applied to a wide range of problems of practical interest, including materials and structures related to hydrogen storage. Theory and computation can be used not only to understand experimental results, but also to guide the search for, and design of, new hydrogen-storage materials.

In the past few years, there have been a number of reviews on hydrogen storage materials with different foci [13–17]. In this chapter, we offer our perspective on the progress of research in hydrogen storage. We do not intend to provide a complete review of the literature, but rather to focus on nanostructure design, with emphasis on computation-based studies. The research is categorized into three parts: (i) nanosized effects on hydrogen storage; (ii) nanostructured materials for hydrogen storage; and (iii) nanobuilding-blocks for novel hydrogen storage materials, as detailed in the following sections.

2 Nanosized Effects in Hydrogen Storage

Metal hydrides, in particular complex hydrides, have been actively studied as hydrogen storage media. However, these hydrides suffer from the fact that hydrogen is held atomically through strong ionic or covalent bonds, making release of hydrogen occur only at high temperatures. Nanoengineering can be used to modify the thermodynamics and kinetics involved in hydrogen release and uptake. For example, ball-milling has been often used to mix the additives and hydrides and to reduce the size of the hydride particles, thereby, increasing the surface area and reducing the diffusion path. We will start by discussing complex metal hydrides and move on to other hydrides.

2.1 Complex Metal Hydrides

The alkali metal aluminohydrides and borohydrides are compounds belonging to a larger class of complex hydrides. In the past, these hydrides were known to liberate copious amounts of hydrogen either by direct thermal decomposition or hydrolysis [18]. The bonding characteristics of these complex hydrides determine that

their dehydriding and hydriding are unfavorable either thermodynamically or kinetically under moderate conditions. As such, the processes were generally considered irreversible and not useful as reversible hydrogen storage materials. This bleak outlook persisted until Bogdanović and Schwickardi demonstrated that $NaAlH_4$ reversibly releases and re-adsorbs hydrogen under relatively mild conditions when doped with Ti-containing compounds [19]. The sodium alanate releases/uptakes hydrogen through a series of reversible decomposition/recombination reactions:

$$NaAlH_4 \rightleftarrows 1/3Na_3AlH_6 + 2/3Al + H_2 \quad (3.7\ \text{wt}\ \%) \qquad (R1)$$

$$1/3Na_3AlH_6 \rightleftarrows NaH + 1/3Al + 1/2H_2 \quad (1.9\ \text{wt}\ \%) \qquad (R2)$$

$$NaH \rightleftarrows Na + 1/2H_2 \quad (1.9\ \text{wt}\ \%) \qquad (R3)$$

The first two combined reactions give a theoretical hydrogen capacity of 5.6 wt% at low to medium temperatures (<250°C), which is considered practically reversible. The remaining 1.9 wt% of hydrogen released in the third step through the decomposition of NaH occurs at temperatures above 400°C, which is considered too high for most technical applications [20]. Clearly, the process couples a series of chemical reactions with solid-state phase transitions that require all elements to be mobile during the reactions. This mechanism is significantly different from that of hydrogen stored in conventional metal hydrides, in which hydrogen atoms are the only mobile species with the metal lattice providing the framework.

The structural change and energetics associated with the creation of the surfaces are expected to have strong effects on the thermodynamics of the complex hydrides and the kinetics of hydrogen release and uptake from either the bulk crystalline phase or nanosized particles. As such, the relative stability of various crystalline surfaces is critical to the size and shape of a particle. Furthermore, the stability of a surface under varying conditions is based on thermodynamics arguments. In the following, we will use $NaAlH_4$ to illustrate the thermodynamic analysis used to predict the shape of a particle. We also relate the surface stability to the ambient condition, including temperature and gas phase compositions.

2.1.1 Thermodynamic Analysis of Complex Hydrides

Considering $NaAlH_4$, a complete dehydrogenation to form Na and Al takes place through Na_3AlH_6 and NaH as reaction intermediates. Conceptually, the alanate consist of three regions: bulk alanates, a gas phase that is in contact with the solid, and an interfacial region with chemical composition $Na_xAl_yH_z$. To prevent $NaAlH_4$ from decomposing, the hydrogen partial pressure and temperature must be kept in a range where the alanate is thermodynamically stable, i.e., the hydrogen partial pressure is sufficiently high and the temperature sufficiently low. At thermodynamic equilibrium of the solid–gas interface, the chemical potentials of all species are equal in each region. For the Na and Al atoms in the system, the large region of

alanate determines their chemical potential. The chemical potential of hydrogen is given by its value in the gas phase of pressure, P, and temperature, T. Therefore, the free energy, Ω, of an alanate surface under a hydrogen atmosphere can be written as:

$$\Omega = G - N_{\mathrm{Na}}\mu_{\mathrm{Na}} - N_{\mathrm{Al}}\mu_{\mathrm{Al}} - N_{\mathrm{H}}\mu_{\mathrm{H}}, \tag{1}$$

where G is the Gibbs free energy of the surface region, $N_{\mathrm{Na}}\mu_{\mathrm{Na}}$ and $N_{\mathrm{Al}}\mu_{\mathrm{Al}}$ are the Gibbs free energies of all Na and Al atoms in the surface region with the chemical potentials of Na and Al equal to those in bulk alanate, and $N_{\mathrm{H}}\mu_{\mathrm{H}}$ is the total Gibbs free energy of all hydrogen atoms in the surface region with a chemical potential equal to that in the gas phase. At a given temperature and pressure, the thermodynamically most stable system minimizes the surface free energy by adapting the stoichiometry of the surface region, i.e., by varying N_{Na}, N_{Al} and N_{H}. Conceptually, this is accomplished by an exchange of Na and Al atoms from the bulk and surface regions of the alanate and by exchanging H atoms between the solid and the gas phases.

For $P_{\mathrm{H}} = 0$ and $T = 0$ with a slab model for the surface, $G \cong E$, Eq. 1 leads to the familiar expression for surface energies, namely:

$$\gamma = \frac{1}{2A}\left(E_{\mathrm{slab}} - E_{\mathrm{bulk}}\right) \tag{2}$$

where γ is the surface energy, E_{slab} is the total energy of the slab, E_{bulk} is the total energy of the bulk system with the same number of atoms as in the slab, and A is the surface area of the unit cell.

The relationship between Eqs. 1 and 2 can be established by the following steps: (i) approximating the Gibbs free energy, $G = E_{\mathrm{el}} + E_{\mathrm{vib}} + E_{\mathrm{other,internal}} + PV - TS$, with the electronic energy, E_{el}, which is often the dominant term; (ii) replacing the surface region by a single slab with the stoichiometry of the bulk phase. The Gibbs free energy of the surface region is then approximately $G \cong E_{\mathrm{el,slab}}$; with the stoichiometry given above and the constraint that the chemical potential of each species is equal to that of the species in the bulk, the term $N_{\mathrm{Na}}\mu_{\mathrm{Na}} + N_{\mathrm{Al}}\mu_{\mathrm{Al}} + N_{\mathrm{H}}\mu_{\mathrm{H}} = G_{\mathrm{bulk}} \cong E_{\mathrm{el,bulk}}$. Normalizing to the surface area, A, and taking into account the fact that a slab has two surfaces, Eq. 1 becomes Eq. 2.

The Gibbs free energy of the surface region is given by:

$$G = E + PV - TS \tag{3}$$

with E being the internal energy. It is assumed that the terms PV and TS are similar for different surface terminations and thus will cancel out. Furthermore, the internal energy is approximated by the total electronic energy of the surface region, as obtained from DFT calculations. This assumption implies that the phonon density of states of the solid does not depend strongly on the surface structure and composition. In particular, the zero-point energies of the various systems are assumed similar and thus can be ignored. Alternatively, these approximations can be corrected to the first-order using linear-response theory [21].

For $NaAlH_4$, the chemical potentials of Na, Al and H, μ_{Na}, μ_{Al} and μ_{H}, are linked through bulk alanate, which serves as a reservoir of Na and Al atoms:

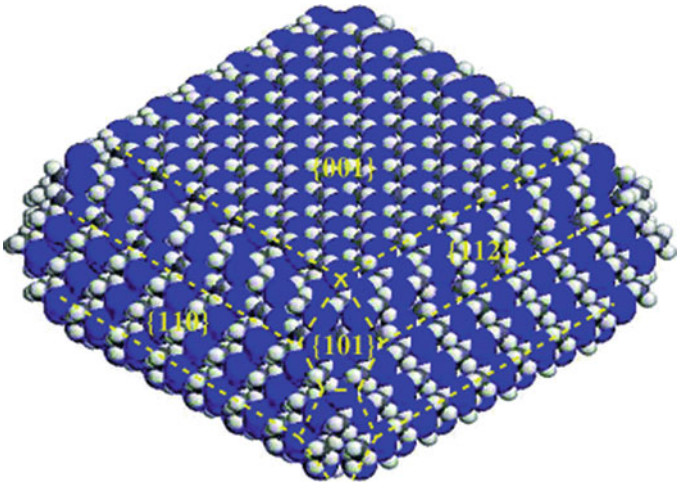

Fig. 3 The predicted equilibrium crystal shape of $NaAlH_4$ determined from the Wulff construction [22]. Reproduced by permission of the PCCP Owner Societies

$$\mu_{Na} + \mu_{Al} + \mu_H = \mu^{bulk}_{NaAlH_4}, \tag{4}$$

where $\mu^{bulk}_{NaAlH_4}$ is the chemical potential of bulk $NaAlH_4$. This term is approximated by the total electronic energy per formula unit of bulk $NaAlH_4$. With these assumptions and approximations, we obtain the gas-surface interfacial free energy:

$$\Omega = E_{slab} - (N_{Na} + N_{Al})\mu^{bulk}_{NaAlH_4} + (4N_{Na} - N_H)\mu_H \tag{5}$$

By normalizing to the surface area, we get the surface free energy:

$$\gamma = \frac{1}{2A}\Omega \tag{6}$$

Using the calculated surface energies for surfaces with different indices, Vegge [22] applied the Wulff construction [23] to predict the shape of a $NaAlH_4$ particle, as shown in Fig. 3. Similar methods were used by Kim et al. to predict the equilibrium shapes of particles for Sc, Ti and their hydrides [24].

The gas phase above the alanate surface contains molecular hydrogen, as well as other hydrogen-containing species. If the pressure is sufficiently low and the temperature sufficiently high, one can neglect intermolecular interactions and treat the pressure dependence using the ideal gas model. To describe the thermodynamic equilibrium of any dehydriding reaction step or the overall reaction, we use the van't Hoff equation to relate hydrogen partial pressure and the enthalpy of the reaction:

$$\ln\frac{P}{P_0} = -\frac{\Delta G^0}{RT} = -\frac{\Delta H^0}{RT} + \frac{\Delta S^0}{R} \tag{7}$$

For a dehydriding reaction that produces a gaseous product, ΔS is always positive, and was estimated to lie in a small range of 100–130 J $K^{-1}(mol\ H_2)^{-1}$ [25].

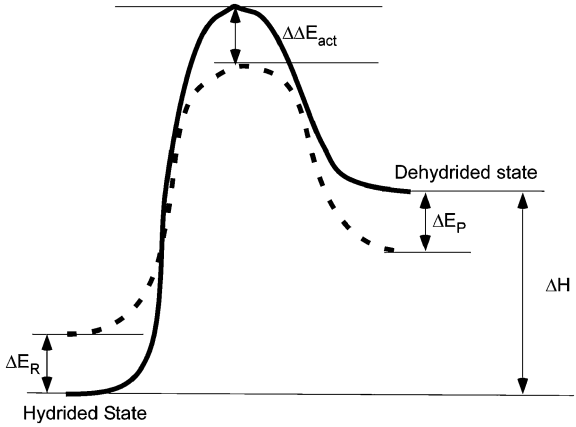

Fig. 4 Schematic potential energy profile for a hydrogen release reaction. The overall reaction enthalpy and activation energy can be manipulated by destabilizing/stabilizing the reactant and product states or adding catalysts

As a result, the equilibrium hydrogen pressure will depend on the enthalpy change of the dehydriding reactions. If the dehydriding reaction is exothermic, we would expect $P > P^0$ all the time, i.e., thermodynamically favoring hydrogen release. On the other hand, dehydriding is endothermic in most cases. As such, a relatively narrow window of 30–78 kJ (mol H_2)$^{-1}$ for ΔH^0 is expected for potential hydrogen storage materials to operate in the temperature range of 300 to 600 K [25]. The challenge is then to identify or design materials that will have a dehydriding/dehydrogenation enthalpy in the range of 30–78 kJ (mol H_2)$^{-1}$. The reaction enthalpy can be modified by using additives to change the hydrided/hydrogenated or dehydrided/dehydrogenated states involved in hydrogen release/uptake reactions. In the following sections, we will use examples to illustrate some of the strategies.

2.1.2 Modifying Sodium Aluminohydrides

The decomposition reaction steps R1 and R2 for releasing hydrogen are significantly endothermic, with the heats of reaction being 37 and 15.7 kJ, respectively [20]. Generally, dehydriding reactions are endothermic and follow a schematic potential energy profile corresponding to the solid line shown in Fig. 4. The hydride releases its hydrogen by going through a transition state with a substantial barrier. There are three states involved in the reaction that can be modified to promote hydrogen release. Based on the potential energy profile, destabilizing the reactant state and/or stabilizing the product state will make the reaction less endothermic, i.e., reducing ΔH, and thereby energetically favor the dehydrided state. The reduction of endothermicity will shift the reaction toward the product state. On the other hand, to improve the kinetics of the reaction, one can introduce catalysts to the system or reduce the size of the hydride particles to lower the barrier of the reaction, as we will discuss in the following sections.

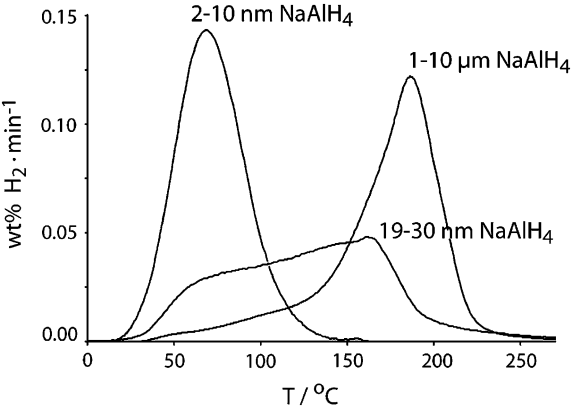

Fig. 5 Temperature programmed desorption profile of H_2 for $NaAlH_4$ supported on carbon nanofiber. Reprinted with permission from [36]. Copyright 2008, American Chemical Society

One or a combination of these approaches may be applied to many hydrides to reduce the hydrogen release temperature and improve the kinetics of the reactions.

For complex metal hydrides, attempts have been made to reduce ΔH by introducing a second cation. Chemically, the decomposition enthalpy of hydrides can be reduced by substituting a cation with a metal of larger ionization potential (IP). The two cations mixed in one hydride are expected to function synergistically to maintain reasonable stability, and at the same time provide a favorable decomposition enthalpy. Extensive DFT calculations showed that bialkali hexahydrides, such as K_2LiAlH_6, K_2NaAlH_6, KNa_2AlH_6, and $LiNa_2AlH_6$, are stable compared to the pure alanates [26, 27]. In fact, $LiNa_2AlH_6$ was synthesized experimentally [28, 29]. Mixed aluminohydrides such as $LiMg(AlH_4)_3$ and $LiMgAlH_6$ were also predicted based on DFT studies, and synthesized and characterized experimentally [30, 31]. Although their overall hydrogen storage performance was not fully examined, some of these compounds exhibit favorable decomposition temperatures.

An alternative approach to modify sodium alanate is to reduce the particle size to the low nanometer regime and maintain the size during hydrogen cycling. In fact, nanosizing effects have been widely exploited in metal hydrides to improve their performances [32–34]. This approach was recently applied to $NaAlH_4$ by supporting $NaAlH_4$ on carbon nanofibers with controlled size ranges: 1–10 μm, 19–30 nm, and 2–10 nm [35, 36]. The activation energies for hydrogen desorption decreased with decreasing particle size, from 116 kJ mol^{-1}, to 80 kJ mol^{-1} and to 58 kJ mol^{-1}, respectively [36]. Figure 5 shows a clear decrease in hydrogen desorption temperature as the size of the particles is decreased. The authors attributed the decrease in activation energies for hydrogen desorption to the expected higher fraction of more open planes, as well as corners and edges exposed on a nanoparticle. The authors also suggested that the rate-limiting step for the nano-$NaAlH_4$ is hydrogen desorption from the particle, in contrast to the case of the bulk samples. Recent studies from the same group showed that the decomposition of the nano-confined $NaAlH_4$ does not go through the Na_3AlH_6

intermediate state [37, 38]. These latest results confirm the Na_3AlH_6 formation mechanism suggested by Balema and Balema [39]. These authors proposed that Na_3AlH_6 is a product of a solid-state reaction:

$$NaAlH_4 + 2NaH \rightleftarrows Na_3AlH_6 \quad \text{(R4)}$$

instead of directly from $NaAlH_4$ by liberating Al and H_2. The fact that no Na_3AlH_6 was detected suggests that reaction R4 is not operative in nano-confined $NaAlH_4$. This could be a result of rapid consumption of Na by other reactions, such as oxidation. Other support materials include mesoporous silica [40] and MOFs (HKUST-1) [41]. These materials were shown to promote the formation of nanoscale $NaAlH_4$ and reduce the hydrogen desorption temperature. In fact, $NaAlH_4$ confined in MOF pores starts to release H_2 at a temperature as low as 70°C [41], similar to $NaAlH_4$ supported on carbon nanofibers [36]. This may suggest that the particles in the two systems have similar sizes.

2.1.3 Other Complex Hydrides

$LiBH_4$ is considered as an attractive candidate for hydrogen storage due to its intrinsically high gravimetric and volumetric hydrogen capacities (18.2 wt%, 121 kg/m^3) and has attracted much interest [42–49]. Unfortunately, the B–H bond in the pure $LiBH_4$ material is extremely strong and only liberates 2% of the hydrogen around the melting point (541–559 K) [42, 43]. Starting from $LiBH_4$, the partial decomposition to $LiH(s) + B(s) + 3/2H_2(g)$ has the standard enthalpy of 100.3 kJ/mol. The highly endothermic decomposition reaction indicates hydrogen release from $LiBH_4$ must occur at elevated temperatures. The experimental results of Züttel et. al showed a significant hydrogen desorption peak started at 673 K and reached its maximum value around 773 K [42, 43]. Nickels et al. attempted to tune the hydrogen desorption temperature by introducing K to $LiBH_4$ and successfully synthesized mixed alkali metal borohydride ($KLi(BH_4)_2$). The new compound has a similar structure to $LiBH_4$ but decomposes at a lower temperature [50].

Another complex hydride similar to $NaAlH_4$ but having an even higher intrinsic hydrogen capacity is $LiAlH_4$. The decomposition of $LiAlH_4$ is believed to undergo similar steps to $NaAlH_4$. The first decomposition step from tetrahedral $LiAlH_4$ to octahedral Li_3AlH_6 is weakly endothermic [51, 52]. The second decomposition reaction from octahedral Li_3AlH_6 to LiH and Al phase was found to be endothermic with ΔH of 25 kJ/mol of H_2. Its dehydriding was observed to occur at 228–282°C, likely due to kinetic limiting steps. Apparently, the decomposition temperature is too high for practical purposes. The decomposition of $LiAlH_4$ is very slow without a catalyst. Adding catalysts results in an enhanced kinetics [53–56].

By introducing the cation of a metal with a high ionization potential, the hydride/hydrogenated state will destabilize, making the enthalpy of the hydrogen release reaction favorable. Another way to tune the overall reaction enthalpy is achieved by incorporating a second species into the reaction to stabilize the

product state, which will also make the overall reaction enthalpy shift toward hydrogen release. Extensive DFT computations have been performed to assess a large number of possible destabilized metal hydrides [25, 57–60]. By assessing the enthalpies of all possible reactions, more than 300 destabilization reactions are predicted to have favorable reaction enthalpies [25]. Wolverton et al. proposed several guidelines to thermodynamically destabilize the metal hydrides in order to design novel hydrogen storage materials [61]. Basically, the enthalpy of the proposed destabilized reaction must be less than the decomposition enthalpies of the individual reactant phases. In addition, if the proposed reaction involves a reactant that can absorb hydrogen, the formation enthalpy of the corresponding hydride cannot be greater in magnitude than the enthalpy of the destabilized reaction.

Vajo et al. examined this strategy by altering the thermodynamics and kinetics of several metal hydrides [62]. The equilibrium hydrogen pressure and reaction enthalpies change with additives that form new alloys or compound phases upon dehydriding. The formation of new phases lowers the energy of the dehydrided state and efficiently destabilizes the component hydrides. A series of experimental explorations have been performed to destabilize the reaction products of $LiBH_4$ and reduce the dehydriding temperatures [49, 62–72].

2.1.4 Structure and Effect of Doped Transition Metal in $NaAlH_4$

In heterogeneous catalysis, nanoparticles have been used in many industrially and environmentally important reactions. As such, they represent one of the earlier applications of nanotechnology before nanoscience and nanotechnology were formally established [73]. Catalysts have been widely exploited in hydrogen storage to improve the kinetics of hydrogen release and uptake in complex hydrides and metal hydrides, following the pioneering work of Bogdanović and Schwickardi [19]. A great number of studies have been devoted to experimentally characterizing alanates, as well as developing new dopants as catalysts to improve the kinetics and cyclability [15, 20, 40, 55, 74–112]. Attempts have been made to elucidate the effect of Ti-based dopants on the structure and hydrogen-storage characteristics. Early results showed that the rates of hydrogen absorption and desorption strongly depend on the level of catalyst doping; the total reversible hydrogen capacity decreases as the Ti-halide doping level is increased. Many types of dopants result in enhanced hydrogen release/uptake kinetics in alanates. Although great progress has been made in characterizing the state of Ti in dehydrided and hydrided materials, an overall understanding of the role of Ti additives in hydrogen release and uptake has still not been achieved.

Many studies indicate that a surface-localized species consisting of a nascent binary phase Ti–Al alloy formed during cyclic dehydriding and rehydriding processes [113–115]. The alloy was investigated in amorphous form by an X-ray diffraction and absorption study [113], as shown Fig. 6a. Combined TEM-EDX and XAFS measurement determined that Ti was atomically dispersed on an Al phase and forms an Al–Ti alloy on the surface of the Al particle, separating from

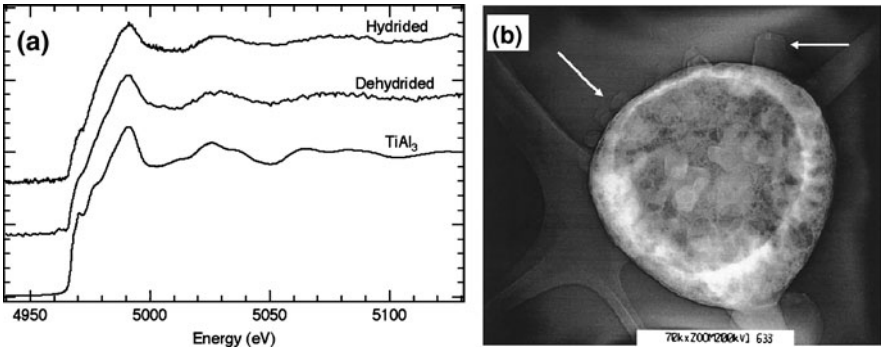

Fig. 6 **a** Ti K edges from $TiAl_3$ and 2 mol % Ti-doped sodium alanate in hydrided and dehydrided states. Reprinted with permission from [113]. Copyright 2004, American Institute of Physics; **b** TEM image of a dehydrogenated titanium doped $NaAlH_4$ sample [114]. Reproduced by permission of The Royal Society of Chemistry

the NaH phase, as shown in Fig. 6b [114, 115]. Based on the thermodynamic stability, $TiAl_3$ is the most likely form after dehydriding Ti-doped $NaAlH_4$. The local structure of these species had Ti–Al and Ti–Ti bond distances of 2.79 and 3.88 Å, respectively. However, directly doped $TiAl_3$ alloy in $NaAlH_4$ was found to be substantially less effective than the Ti halides [116].

Many experimental measurements established that highly dispersed Ti in a predominantly Al phase plays an important role in hydrogen uptake and release processes [78, 81, 94, 117]. On the other hand, there is limited experimental data to support the suggestion that the Ti hydrides formed in the process will catalytically enhance dehydriding and rehydriding processes [39, 83, 86, 118]. Although extensive experimental studies have been performed on the Ti-doped $NaAlH_4$ system, the mechanism by which the $NaAlH_4$ system is activated in the presence of a small amount of Ti is still not well understood.

First of all, the Ti is unlikely to simply act as a classic catalyst assisting the conversion between hydrogen atoms and molecules at the solid-state surface. There is a strong thermodynamic driving force for Ti to form a hydride in the presence of hydrogen. Therefore, Ti was proposed to play a role in improving the transport of mobile species, such as AlH_3, to the catalytic site and further make AlH_3 dissociate into Al and H_2 [119, 120], in addition to the enhancement of bond-breaking and bond-forming processes. On the other hand, both hydriding and dehydriding involve complex phase transitions of NaH and $Al \leftrightarrow Na_3AlH_6 \leftrightarrow NaAlH_4$. Different local structures and/or chemical states of Ti may accompany the transformation process. However to accurately determine the structures and location of Ti in such a complicated system and follow it during the hydriding/dehydriding process is extremely challenging to the available experimental techniques. In this aspect, DFT-based first-principles methods are advantageous.

Several theoretical studies have been performed to focus on substitution of Ti for Al and Na atoms in Ti-doped $NaAlH_4$ bulk and surfaces. Substitution of Ti for Al was shown theoretically to be the preferred location in bulk $NaAlH_4$ [121–123]. Ĭñiguez et al. studied the structure, energetics, and dynamics of pure and Ti-doped sodium alanate ($NaAlH_4$), focusing on the possibility of substitutional Ti doping in the bulk [124]. These authors optimized several possible structures for the substitution of Al and Na by Ti, accompanied by neighboring vacancies using the DFT plane-wave method implemented in CASTEP. Their results showed that doped Ti prefers to substitute for Na and further attract surrounding hydrogen atoms, softening and/or breaking the Al–H bonds. The same group of authors extended their study to determine the location of Ti [125]. These later results showed that Ti prefers to be on the surface, substituting for Na, and attracting a large number of H atoms to its vicinity. They predicted that a $TiAl_n$ ($n > 1$) structure might form on the surface of the sodium alanate. On the other hand, this process would cost an energy of 1.7 eV and is, therefore, not likely to happen. However, Løvvik et al. also suggested that substitution of Ti in bulk $NaAlH_4$ is less favorable than that near surface or defect positions. On the $NaAlH_4$ (001) surface, DFT calculations by Yildirim and Íñiguez showed substitution of Ti for Na is the preferred site [125] whereas Løvvik and Opalka found substitution of Ti for Al is more favorable [122, 123]. The difference was attributed to the different reference states used in energy calculations. Although thermodynamic stability of local structure can determine the possible sites of Ti, the improvement of kinetics remains unclear.

Doping with $TiCl_3$ was believed to result in vacancies in $NaAlH_4$ and was simulated by generating Na-vacancies next to Ti [126, 127]. The calculated results show that Na-vacancies play a larger role in reducing hydrogen desorption energies. Na-vacancies lead to a lower hydrogen desorption energy (0.4 eV/H_2) than 0.9 eV/H_2 in the substitutional model. In addition, Vegge's calculations revealed that Na-vacancy formation energies were significantly reduced when Ti is doped in $NaAlH_4$ surfaces [22].

We approached the problem based on a surface model of $NaAlH_4$ and proposed an alternative mechanism based on the surface interstitial complex structure that we identified in Ti-doped $NaAlH_4$ (001) and (100) surfaces [128–131]. This is different from many other computational studies that adopted bulk $NaAlH_4$ models and focused primarily on substitutional modes of doping. The resulting local structures after doping the surface interstitial sites in both surfaces are very similar [128, 129], as shown in Fig. 7. Our results show that the hydrogen desorption energies from many positions of $TiAl_3H_x$ are reduced considerably compared with that from the corresponding clean, undoped $NaAlH_4$ surfaces. The almost invariant local environment surrounding Ti during dehydriding makes the $TiAl_3H_x$ complex a precursor state for the formation of experimentally observed $TiAl_3$ after dehydriding Ti-doped $NaAlH_4$ [113]. Furthermore, we showed that the $TiAl_3H_{12}$ complex has an extended effect beyond locally reducing the hydrogen desorption energy. It also facilitates hydrogen desorption at a reduced desorption energy by either transferring the hydrogen to $TiAl_3H_x$ or by reducing the hydrogen

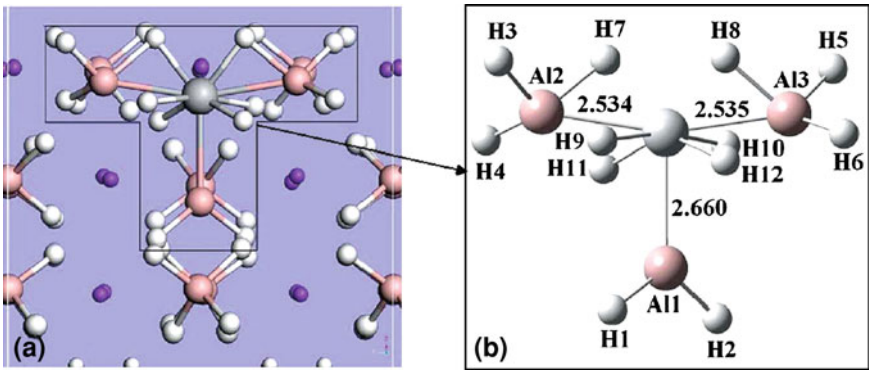

Fig. 7 **a** DFT-GGA relaxed structure of Ti-doped $NaAlH_4$(001) with Ti in the surface interstitial site. **b** Detailed local structure of the $TiAl_3H_{12}$ complex shown in (**a**). Reproduced from [128]

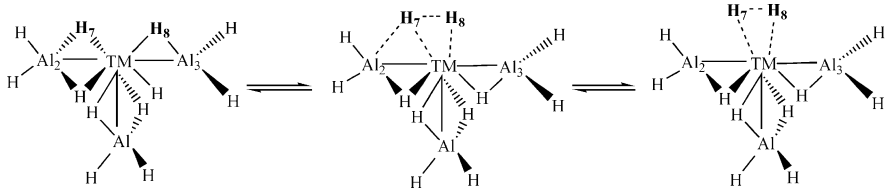

Fig. 8 A proposed ligand exchange mechanism involved in dehydriding and hydriding of transition metal doped $NaAlH_4$. Reproduced from [131]

desorption energy in neighboring AlH_4^- by linking these AlH_4^- units with the complex structure. Our predicted interstitial $TiAl_3H_x$ structure was supported by a recent combined Ti K-edge EXAFS, Ti K-edge XANES, and XRD study of $TiCl_3$-doped $NaAlH_4$ by Baldé et al. [78]. These authors observed that the interstitial structure accounts for more than 70% of all Ti doped in $NaAlH_4$.

The general consensus of the DFT studies of Ti-doped $NaAlH_4$ is that Ti attracts surrounding H atoms, accompanied by breaking the Al–H bonds and forming Ti–H bonds [125, 128, 129]. During the recharging state, transition metals should assist in breaking the molecular hydrogen bond but not prevent the hydrogen atoms from migrating to Al atoms. Based on extensive computational studies, we proposed that a dihydrogen complex is formed in both dehydriding and hydriding processes. In fact, both dehydriding and hydriding can be viewed as ligand exchange between H–H and Al–H, as shown in the scheme in Fig. 8 [131]. Based on stability and calculated hydrogen desorption energy from the $TMAl_3H_{12}$ structures, we concluded that the 18-electron rule is applicable in understanding the variation of binding strength between active site and ligands (H–H and Al–H bonds). Our analysis of electronic structure revealed that electron transfer from d-orbitals of TM to σ^* antibonding bonds plays an important role in hydrogen release and uptake of $NaAlH_4$ [131]. This interaction mechanism between TM and

$NaAlH_4$ can be ascribed to Kubas-type interaction [132], i.e., metal coordinating with σ-bonds to form complexes. In fact, electron transfer from d-orbitals to σ^* bonds of H_2 was also found in hydriding of Ti-doped Al surface structures according to this interaction mechanism [133, 134]. Very recently, Ljubić and Clary confirmed this model by DFT and CCSD(T) calculations for Ti(Sc)-2Na-AlH_4 clusters [135]. They showed that the barrier (10–20 kJ/mol) for H_2 release is reduced considerably with respect to that ($\sim$120 kJ/mol) of the pure $NaAlH_4$.

Based on the above analysis, we can predict the effective catalysts that will improve the performance of complex metal hydrides. In the case of $NaAlH_4$, the early TMs may be more effective than the late TMs in promoting hydrogen release and uptake. In fact, many transition metals have been assessed for their activity in dehydriding and rehydriding of $NaAlH_4$, and among them, Sc, Ti, Zr, Ce, and Pr were shown to be effective [84, 117, 136]. Furthermore, doped transition metal cations reduce to a lower oxidation state, which is favorable for an electron donation from the occupied σ orbitals of Al–H and H–H to transition metal d-orbitals. A transition metal in a higher oxidation state has a higher formal charge and favors the electrostatic interaction between the metal and σ bonding molecules. In experiments, many different precursors, $TiCl_3$, $Ti(OBu^n)_4$, $TiCl_4$, $TiBr_4$, and TiF_3, have been used to examine the catalytic effect [98]. These extensive studies have identified that zero-valence Ti particles are dispersed in the Al phase after hydrogen cycling. Thus, reduction of Ti is expected to occur during the initial doping process such as ball-milling.

In contrast, a different interaction mechanism was found to be operative in Ti-doped $LiBH_4$ surfaces [47]. Although the most stable structures in Ti-doped $LiBH_4$ are similar to those in Ti-doped $NaAlH_4$, the bond-activation by doping Ti into $LiBH_4$ is much less dramatic than in $NaAlH_4$. Our analysis showed that the bond-activation difference can be attributed to the inability of back-donation of electrons from the d-orbitals of Ti to antibonding orbitals of B–H bond. Based on the analysis of structural stability, the symmetry-adapted occupied orbital overlap between d-orbitals and B–H bonding orbitals was found to play an important role in stabilizing structures. This structure promotes hydrogen desorption locally but does not show an extended effect, as in the case of Ti-doped $NaAlH_4$. Consequently, the amount of Ti needed to achieve a significant reduction of hydrogen desorption energy in $LiBH_4$ would be significantly higher than in $NaAlH_4$, consistent with the experimental observations [66, 68, 137].

In summary, the understanding of the interaction mechanism between catalyst and host material will help screen the catalysts that improve performance of the complex hydrides as hydrogen storage media. Clearly, a complicated mechanism is involved in the heterogeneous processes because of phase transition and mass transport. Both experimental measurements and theoretical studies on the catalytic effect of Ti involved in these dynamic processes have been challenging. A recent hydrogen–deuterium scrambling experiments showed that the mass transport of heavy species (NaH or AlH_3) may be rate-determining steps in dehydriding $NaAlH_4$ [85]. Using first-principles DFT simulations, Gunaydin et al. identified that the Al mass transport mediated by AlH_3 vacancy has the lowest barrier of

mass transport, but still is higher than that for the bond-breaking steps [138]. However, the effect of the doped transition metal in mass transport and phase transition remains unclear. A first-principles dynamics simulation may be needed to address the questions involving bond-breaking and making, mass transport, and phase transition.

2.2 Magnesium Hydrides

Magnesium is an attractive and promising material for hydrogen storage applications due to its high hydrogen capacity (7.7 wt%), low cost, and being rich in natural abundance. However, three major problems hamper its commercial usage as a hydrogen storage material. First, the decomposition energy is high, at 75 kJ/mol H_2 [139, 140], which corresponds theoretically to an equilibrium temperature with 1 bar H_2 pressure of 288°C. Kinetic limitations push the desorption temperature to at least 300°C to reach 1 bar H_2 pressure. Second, the hydriding and dehydriding rates are very slow at room temperature, mainly due to the slow diffusion of hydrogen atoms through the hydrides. Third, the hydrogen molecule does not readily dissociate on the Mg surface to generate hydrides for recharging. In fact, these phenomena are common for the main group metals, as reflected by the fact that the enthalpies of formation of the hydrides are usually very large. Catalysts can be added to assist breaking the H–H bond for the recharging phase. The hydrogen atoms generated at the catalytic center will be transferred to Mg sites through hydrogen spillover. Both theoretical and experimental studies have been performed to explore the effectiveness of hydrogen spillover to recharge Mg using a palladium-based catalyst [141–144].

During the past two decades, many experimental methods have been developed to lower the desorption temperature and increase the rate of sorption/desorption. An example is the formation of the complex hydride of Mg_2NiH_4 [145], which resulted in a lowered sorption temperature of $\sim$200°C. However, the hydrogen capacity is significantly reduced, to 3.6 wt%, through this alloying process.

Nanostructured materials have been exploited to improve hydrogen sorption properties from magnesium hydrides. Hydrogen sorption properties of magnesium were greatly improved by combining the material with nanostructures through chemical/physical synthesis [146–149] or high-energy ball-milling with additives [150–156]. The improved sorption kinetics can be ascribed to the increase of the specific surface area, the decrease of diffusion path lengths, and change of electronic structure properties. Despite many improvements, hydrogen desorption temperature remains too high for practical applications.

The size effect of nanoparticles on the hydrogen interaction in MgH_2 was analyzed by Wagemans et al. using ab initio Hartree–Fock (HF) and DFT calculations [157]. These authors found that both magnesium and magnesium hydride become less stable with decreasing cluster size, notably for clusters smaller than 20 magnesium atoms. However, magnesium hydride destabilizes more strongly

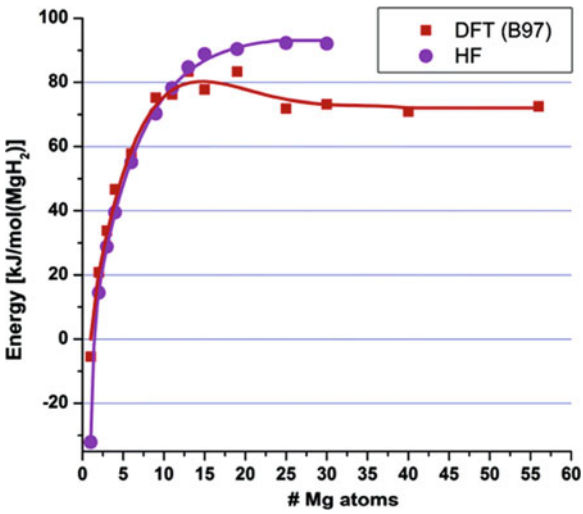

Fig. 9 Calculated average hydrogen desorption energy from Mg_nH_{2n} for clusters with different number of Mg atoms. Desorption energy was normalized to MgH_2. Reprinted with permission from [157]. Copyright 2005 American Chemical Society

than magnesium. As a result, the hydrogen desorption energy decreases significantly when the crystal grain size becomes smaller than 1.3 nm, as shown in Fig. 9. For instance, an MgH_2 crystallite size of 0.9 nm corresponds to a desorption temperature of only 200°C. This predicted decrease of the hydrogen desorption temperature is an important step toward the application of Mg as a hydrogen storage material. Cheung et al. simulated the hydrogen desorption/sorption processes using a reactive force field method and focused on the size dependency of MgH_2 and Mg nanoparticles [158]. They predicted that the heat of MgH_2 formation is very close to that of the bulk structure for clusters larger than 2 nm. It is expected that an ionic bond exists between Mg and H atoms in MgH_2 structures due to the large difference (0.7) of their electronegativities. A MgH_2 nanostructured particle exposes its highly reactive edges and corners on its surface. Therefore, fabricating and maintaining a small size nanoparticle (less than 2 nm) in hydrogen storage applications using MgH_2 is very challenging. Mechanical milling of MgH_2 leads to particles with sizes of 20–300 nm [159]. Consequently, the MgH_2 particles produced by ball-milling are not expected to show any significant difference in thermodynamic properties from the bulk crystalline particles. Small size (2–5 nm or smaller) of the Mg crystallites have been synthesized in nanoporous carbon by infiltration [147].

A DFT calculation of the electronic structure and total energies of MgH_2 nanoclusters that are interacting with transition metal dopants has been carried out to understand the catalytic effect of transition metals (Ti, V, Fe, and Ni) in dehydriding of MgH_2 nanoclusters by Larsson et al. [160]. The authors reported both the effect of doping transition metal on average and single-site desorption energies. Their results showed that the doped transition metal did not change the

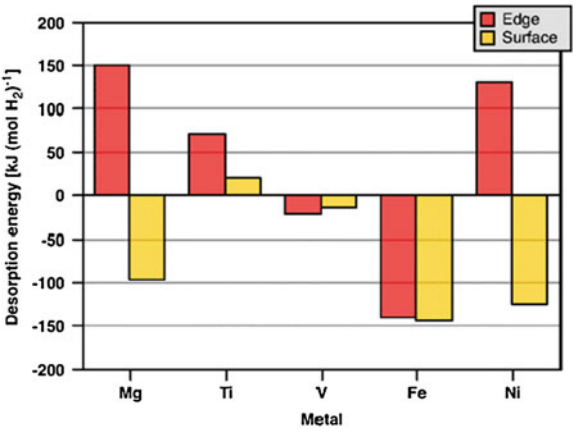

Fig. 10 Calculated single-site hydrogen desorption energies for $Mg_{30}MH_{62}$ clusters at two different surface sites. Reprinted with permission from [160]. Copyright 2008, National Academy of Sciences, U.S.A

average desorption significantly but has a dramatic effect on the single-site desorption energy, as shown in Fig. 10, which reveals the local effects of the transition metal catalysts. In MgH_2 nanoclusters, the removal of hydrogen bound to edge-site Mg atoms costs energy, whereas the process is exothermic for the surface Mg atoms. This is consistent with previous studies that nanostructuring can by itself lower the temperature required for the onset of hydrogen release [157, 158, 161–163], even without the addition of catalysts. Most strikingly, doping Fe or Ni led to the negative removal energies of H atoms from both of the surface sites. The authors argued that this kind of exothermic dissociation might lower the minimum temperature needed to initiate hydrogen desorption, especially because an application of the Hammond–Leffler postulate suggests that the corresponding activation energies will be lower as well. They propose that the transition metal, in particular, Fe, is mobile and remains at the Mg/MgH_2 interface to catalyze dehydriding. On the other hand, searching for a method to stabilize the nanosized magnesium hydrides particles as well as highly active catalysts remains a challenge for implementing magnesium hydrides in practical hydrogen storage.

3 Nanostructured Materials for Hydrogen Storage

High surface porous materials have been used as gas separation and storage materials for a long time. Carbon-based nanostructures, including nanotubes and amorphous carbon have been widely studied for their hydrogen storage properties [14, 164–166]. Metal–organic frameworks (MOFs) are a novel class of nanoporous materials that are built with metal ion clusters linked by rigid organic linkers. The potential of using such materials as hydrogen storage media was first demonstrated by Rosi et al. [9]. Recently, a new family of three-dimensional covalent organic frameworks (COFs) were synthesized and explored for hydrogen storage [167].

Both MOFs and COFs have shown exceptionally high hydrogen capacities because of their large surface areas and porous structures [168, 169]. In COFs, the organic building units are held together by strong covalent bonds (C–C, C–O, B–O, and Si–C), which replace the heavy metal ions in MOFs materials. Therefore, COFs-based materials have not only a larger gravimetric capacity of hydrogen, but also show a high thermal and architectural stability. Hydrogen stored in this type of material remains molecular. According to the thermodynamic analysis by Bathia and Myers, a heat of adsorption of 15.1 kJ/mol is required for an adsorbent to remain attractive to hydrogen at ambient temperature [170]. On the other hand, MOFs and COFs have a weak binding toward H_2 (4–7 kJ/mol) [167, 171, 172]. Hydrogen storage in these materials with significant capacity can only occur at cryogenic temperatures ($\sim$77 K).

High surface area and pore volume form the basis of MOFs and COFs materials as hydrogen storage media. The working temperature is limited by their weak interaction with dihydrogen. On the other hand, the flexibility and diversity of MOFs' and COFs' structures allow some improvements for hydrogen storage at ambient conditions by increasing the affinity of dihydrogen toward host materials. In elastic neutron scattering experiments and grand canonical Monte Carlo (GCMC) simulations suggest that the open metal clusters within MOF are the preferred binding sites at low pressures while organic linkers play a more crucial role at higher pressures [9, 173]. This was attributed to the fact that, although the absorbent sites in the organic linker have lower binding energies, a much greater number of such sites produce an additive effect and resulted in increased H_2 loading [174]. Consequently, many studies have been reported to enhance H_2 binding strength with MOFs and COFs by modifying the metal ions or organic linkers.

The nature of dihydrogen interaction with the metal ions in MOF materials can be understood by examining similar metal-modified carbon-based materials. In the latter case, the metal cation interacts with H_2 through electrostatic interaction and possibly electron transfer as described in the Dewar, Chatt, and Duncanson (DCD) model [175]. For early transition metals, electron transfer is expected to be the main contributor to H_2 interaction with host sites [176]. The main group metals and late transition metals rely on electrostatic interaction to bind H_2 [177]. The metal ions in MOFs are expected to behave similarly to the metal ions in the metal-modified carbon-based materials. However, the local environment of metal ions may lead to a different situation from the metal-modified carbon-based materials. Monte Carlo simulations were performed for hydrogen interaction in the MOF structure of $\left[In_3O(C_{16}N_2O_8H_6)_{1.5}\right]NO_3$ [178]. In this case, hydrogen interacts with the MOF through three principle attractive forces: van der Waals, electrostatic, and induction. The DFT study of Zhou and Yildirim on the binding of H_2 on Mn cation in Mn_4Cl-MOF structure (Fig. 11) showed that the major contribution to the overall binding arises from electrostatic effects [179]. The interaction strength was also found to depend on the local environment, including the spin-state of the metal ion and H_2 orientation. Obviously, a single system cannot represent all possible hydrogen interaction mechanisms in MOFs.

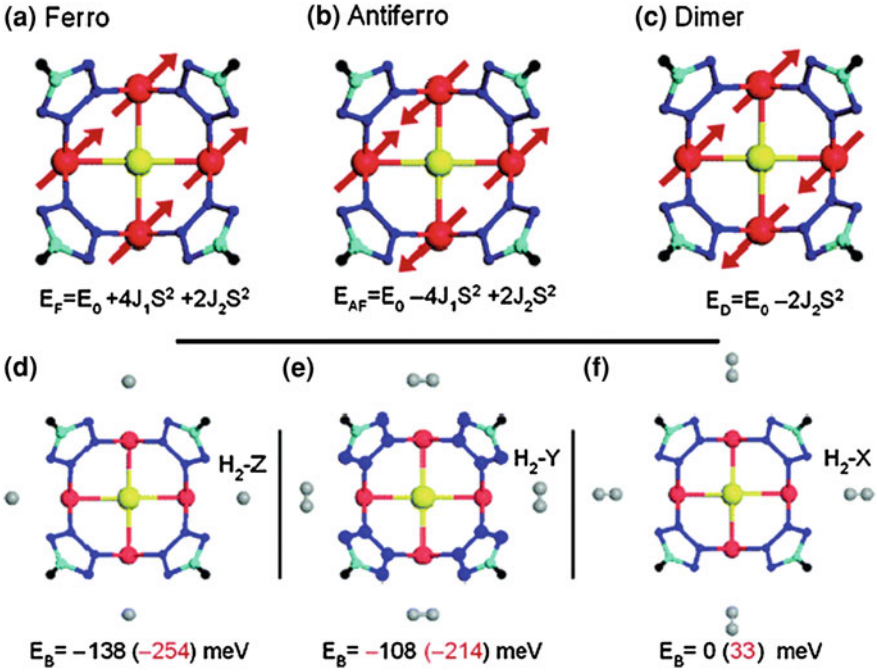

Fig. 11 *Top* view of the Mn_4Cl-MOF cluster with three magnetic configurations and their energies in terms of nearest (J_1) and next-nearest (J_2) exchange interactions. The bottom panel shows $H_2-Mn_4Cl-MOF$ cluster for three different H_2 orientations. The H_2 binding energies (E_B) and pure Coulomb contributions (in parentheses) are also given. Reprinted with permission from [179]. Copyright 2008, American Chemical Society

In general, terminal ligands are bound to metal centers by a Lewis acid/base interaction. The open metal site may be formed by removing these terminal ligands without destruction of the framework. Mostly, these exposed metals are divalent cations, electron deficient, and expected to form dihydrogen σ complexes. By generating frameworks bearing open metal coordination sites, it is possible to increase the H_2 affinity of the surface, giving rise to a higher storage capacity at room temperature [172, 180, 181]. For example, it was reported that the exposed Mn^{2+} coordination sites within $Mn_3[(Mn_4Cl)_3(BTT)_8]_2$ contribute to its record uptake of 1.49 wt% and 12.1 g/L at 298 K and 90 bar [172]. By examining various metal ions in MOF structure, Zhou et al. provided some insight into the increased binding strength of H_2 in MOFs [182]. These authors performed DFT calculations on a series of isostructural MOFs, M_2(dhtp) (M = Mg, Mn, Co, Ni, Zn, and dhtp = 2,5-dihydroxyterrphthalate). They reported that the H_2 binding strength has the trend, $Zn^{2+}(4.43\ kJ/mol) < Mn^{2+}(4.70\ kJ/mol) < Mg^{2+}(5.99\ kJ/mol) < Co^{2+}(6.28\ kJ/mol) < Ni^{2+}(7.33\ kJ/mol)$. These results suggest that the relative strength of the metal center may be empirically correlated with the ionic radius of cations in the same coordination environment. Sun et al. also studied the

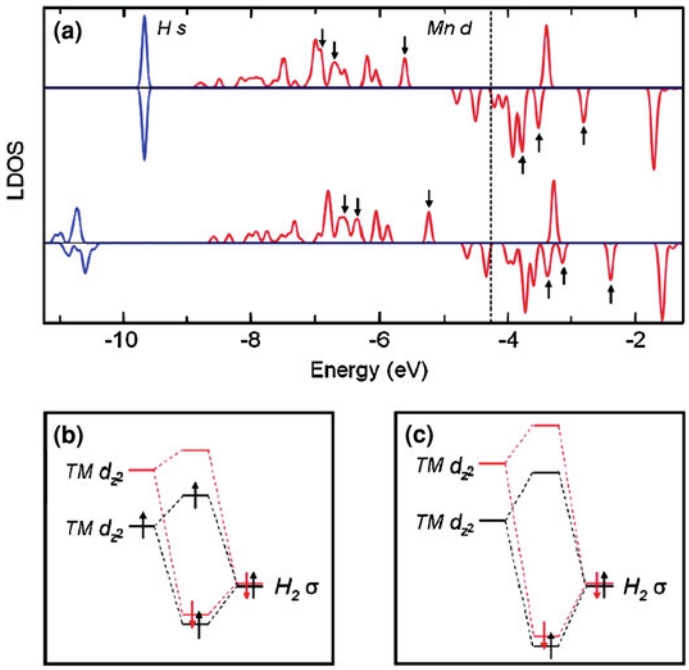

Fig. 12 **a** Local spin density of states on Mn d and H s before (*upper*) and after (*lower*) H_2 adsorption. **b** Schematic diagram illustrating the orbital interactions between TM dz^2 and H_2 σ in the Mn − and Cr − MOFs. Reprinted with permission from [183]. Copyright 2007, American Chemical Society

binding of H_2 in MOFs using a different set of transition metals [183]. Based on the analysis of electronic structure change before and after H_2 adsorption on the Mn site of Mn-doped model MOFs (Fig. 12), these authors predicted that doping with an early transition metal would lead to stronger H_2 binding. They further calculated the binding energies of 8.4, 10.4, 21.9, 34.6, and 46.5 kJ/mol for Mn, Sc, Ti, and V doped MOFs. Clearly, early transition metals in MOFs have a larger binding energy than late ones. The authors proposed a special Kubas-type interaction and attributed the orbital interactions between a TM center and an approaching dihydrogen to four key factors: (1) the separation of the H_2 σ level and the TM d levels, which decreases when the atomic number increases; (2) the splitting of the spin-up and spin-down d-levels which is reflected by the magnetic moment of the TM center; (3) the position of the most responsive d-levels to the approaching H_2 which is determined by the crystal field splitting of the d-orbitals according to the local symmetry of the TM center; and (4) the occupancy of the responsive d levels which is determined by the number of valence electrons and the oxidation states.

Both experimental and theoretical studies revealed that the aromatic rings on the organic linkers play an important role in H_2 adsorption, particularly at a higher

hydrogen pressures [184]. However, the interaction between H_2 and organic linkers, van der Waals and induction interactions, are generally too weak to have a significant impact on increasing the binding energy of H_2 molecule to host materials [185]. The dispersive interactions are a challenge for DFT-based approaches. On the other hand, the size of MOFs is too big for the wave-function-based ab initio methods. Han and Goodard developed a first-principles-derived force field to describe nonbonding interaction involved in hydrogen interactions in MOFs [186]. This new potential represents a significant improvement from Lenard-Jones empirical force field in predicting hydrogen storage properties in high surface area porous materials, including MOFs and COFs. However, a stronger type of interaction (electrostatic and orbital overlap) must be evoked to improve the binding energy of H_2 with organic linkers. Modification of the aromatic linkers has been considered. The simulation results based on the new potential are in good agreement with the experimental results [184, 187].

A series of GCMC simulations with different organic linkers were performed to examine the doping effect of Li cations based on this force field potential [188].

As shown in Fig. 13, doping Li in MOFs increases hydrogen uptake at room temperature significantly. At 300 K, Li-doped MOF-C30 was found to absorb 3.89 wt% at 20 bar and 4.56 wt% at 50 bar, which is the highest reversible hydrogen storage capacity at room temperature reported so far. In contrast, hydrogen storage capacities of pure MOF-C30 are calculated as 0.25 and 0.56 wt% at the corresponding pressures and temperature. Other organic linkers doped with Li also showed increased hydrogen capacities over unmodified MOFs. The increased hydrogen capacity can be attributed to increased electrostatic interactions. In Li-doped MOF structures, Li is attracted to the high electron affinity of aromatic linkers and becomes a positive Li cation. The cooperative electrostatic interaction to H_2 from metal ion clusters and doped Li ions leads to a strong binding toward H_2 molecules. Indeed, the Li-doped MOF-C30 exhibited a high binding energy of 16.7 kJ/mol, which is significantly attractive to H_2 at ambient temperature. Therefore, these computational studies established that doping Li in MOFs is a very effective way to improve the binding strength of H_2 within MOFs. The prediction was confirmed by Mulfort and Hupp, who used chemical reduction methods to obtain Li-doped MOF and found that the hydrogen adsorption capacity nearly doubled [189]. Such improvement of binding strength between H_2 and Li-doped MOFs was also confirmed by other ab initio calculations and GCMC simulations [190, 191]. Han et al. further predicted that this doping effect also can increase the binding energies of H_2 with COF material to achieve the hydrogen storage target at room temperature [10].

Klontzas et al. explored another modification for organic linkers by substituting a terminal hydrogen atom with a Li atom and forming a modified Li alkoxide group [192], as shown in Fig. 14. Results from ab initio calculations showed interaction energies between hydrogen molecules and the modified group are up to three times larger than H_2 with unmodified MOFs. They obtained a very promising result, 4.5 wt% hydrogen storage at room temperature [192].

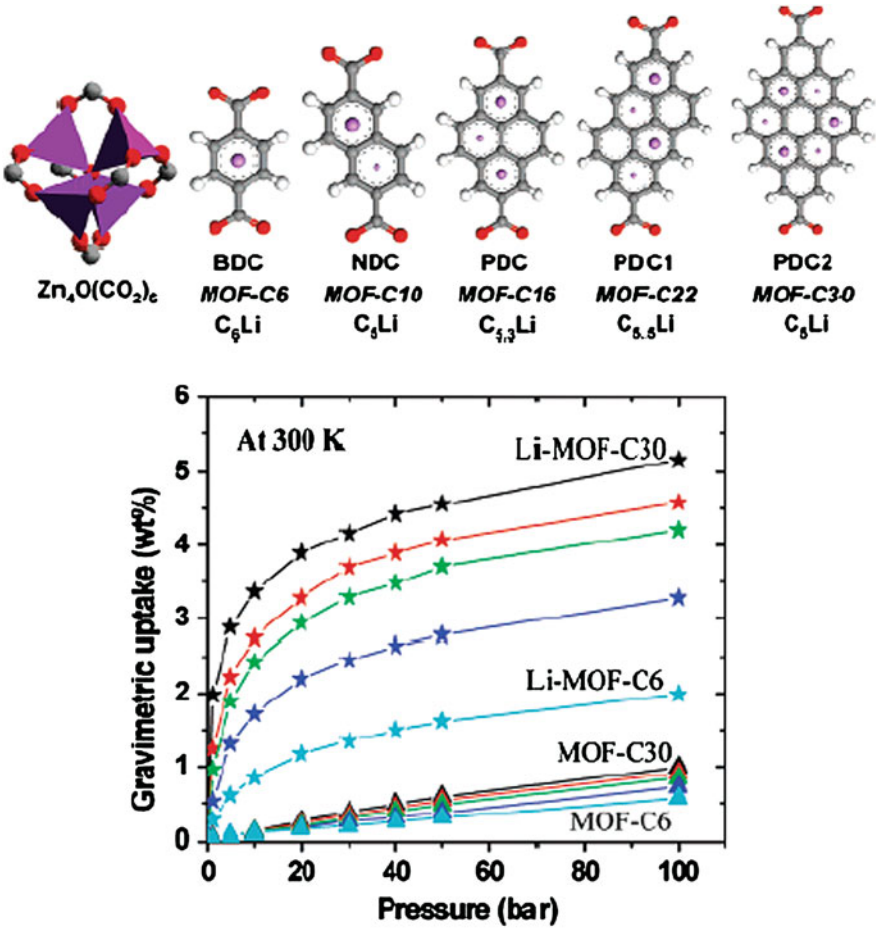

Fig. 13 The building blocks (metal oxide center and Li-doped organic linkers) for MOF structures (*upperpanel*) and predicted H_2 adsorption isotherms at 300 K for assembled MOFs (*lower panel*). Reprinted with permission from [188]. Copyright 2007, American Chemical Society

Similarly, Li-doped in covalent organic frameworks also improves their hydrogen capacity at room temperature [193, 194]. First-principles calculations showed that doping Li in the COF materials led to a higher gravimetric adsorption capacity at T = 298 K and p = 100 bar, 6.84 and 6.73 wt% for Li-doped COF-105 and COF-108. A multiscale theoretical method combined with the first-principles calculation and GCMC simulation was performed to investigate the hydrogen adsorption properties in undoped and Li-doped COF-202. The GCMC simulation predicted that the total gravimetric and volumetric uptakes of hydrogen in the Li-doped COF-202 could reach 4.39 wt% and 25.86 g/L at T = 298 K and p = 100 bar. In contrast, the maximum H_2 gravimetric and volumetric uptake of

the undoped COF-202 are only 1.52 wt% and 8.08 g/L at $T = 298$ K and $p = 100$ bar.

Experimentally, significant effort has been made to understand and improve binding strength. Many MOFs are found to have a large space between their links. For example, the distance between phenylene faces in MOF-5 is measured to be 15 Å in diameter [9]. There would be an unused void volume at the center of these pores. In order to increase the attractive interactions between the wall and hydrogen, one would reduce the size of the pore. A smaller pore facilitates the overlapping of potentials from two or more linkers, thereby creating a synergy toward binding the hydrogen molecule. Dinca et al. observed H_2 binding energies of up to 9.5 kJ/mol by increasing van der Waals contact area associated with a very small pore size [172]. Four-fold catenated IRMOFs also have been reported to have a larger hydrogen capacity at room temperature and 48 bar [195, 196].

4 Nanobuilding-Blocks for Novel Hydrogen Storage Materials

Inspired by the early work on the use of carbon nanotubes for hydrogen storage at room temperature [164], carbon nanotube materials have been extensively investigated as hydrogen storage media [14]. Some studies showed that carbon-based materials can store a large amount of hydrogen molecules since they contain defect structures that act as trapping sites [197]. Very different hydrogen storage values between 0.25 and 56% were reported under various experimental conditions for carbon nanotube materials [164, 198–201]. Later, it was found that hydrogen storage of > 1.0 wt% was practically impossible to achieve and higher values were possibly the result of measurement errors due to contamination of the analysis gas with water [202, 203]. Theoretical studies also confirmed that high hydrogen content in the pure carbon nanotubes cannot be achieved through physical sorption [204]. On the other hand, Kim et al. studied the hydrogen storage properties of multiwalled carbon nanotubes (MWCNTs) with Ni nanoparticles at moderate conditions of 340–520 K and 4 MPa [205]. Hydrogen uptake up to 2.8 wt% was achieved under these conditions. In fact, other carbon-based materials (activated carbon, and graphite nanofibers) modified by some metals showed increased hydrogen storage capacity [205–208].

For pure carbon-based materials, a low hydrogen storage capacity actually originates from the small binding energy between hydrogen molecules and carbon porous materials. The interaction with carbon nanotubes or carbon fullerenes is interpreted as instantaneous transition dipole or dispersion interaction, which is very weak, on the order of a few kJ/mol. Modification by metals results in increased hydrogen storage capacity, which may be attributed to stronger binding, resulting from electrostatic interaction between the hydrogen molecule and metals. The binding energies between hydrogen and metal are really dependent on reactivity and structural properties of metal clusters.

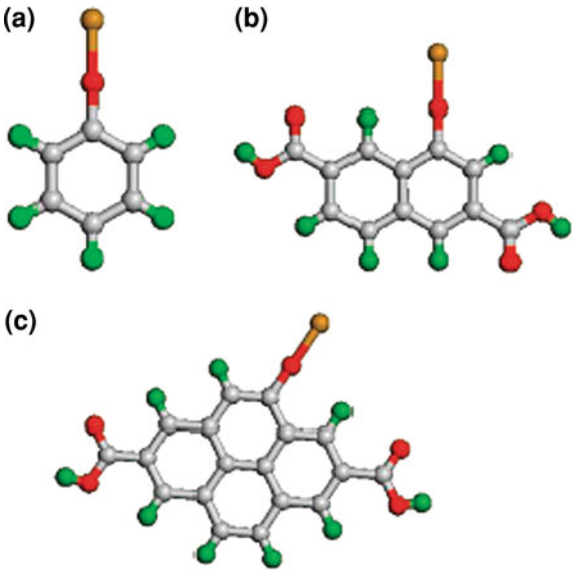

Fig. 14 The modified orgianic linkers. (**a**) Li-alkoxide-benzene, (**b**) Li-alkoxide-anphalene-dicarboxylate (IRMOF-8 linker), and (**c**) Li-alkoxide-pryene-dicarboxylate (IRMOF-14 linker). Reprinted with permission from [192]. Copyright 2008, American Chemical Society

In order to make use of porous carbon materials with high surface areas and improve the weak binding situation, chemists considered metal/transition metal coating of carbon nanotubes and fullerenes. In the following section, we will discuss computational studies on metal/transition metal-coated carbon-based materials, focusing on two important topics: hydrogen capacity and binding energy between hydrogen and metal.

In order to increase hydrogen storage capacity and binding energy of hydrogen, many metals, including alkali metals, alkali earth metals, and transition metals, were used to coat carbon-based materials. Yildirium and Ciraci performed the DFT calculations for a single Ti coated on a single-walled nanotube (SWNT) which could bind up to four hydrogen molecules [209]. The first H_2 adsorption is dissociative with no energy barrier whereas the other hydrogen molecules are adsorbed physically with slightly elongated H–H bonds. The calculated binding energy was 0.13 eV/H_2, which is 4–5 times stronger than dispersion force between hydrogen molecules and SWNT. At a high Ti coverage, SWNT can strongly adsorb up to 8 wt% hydrogen. Later, they further reported computational work on 3d transition metal-decorated C_{60} for hydrogen storage [210]. For early transition metals, the average binding energy of H_2 molecule is 0.3–0.5 eV/H_2 and the maximum hydrogen storage was predicted to be 9.0 wt% [176]. Late transition metals such Fe, Co, and Ni, do not bond to the C_{60} cluster. However, transition metals tend to form clusters on C_{60} instead of uniformly distributing because the binding energy of the nanoparticle is stronger than between TM and C_{60} [211]. In the case of Ti (Fig. 15), the binding energy of nanoparticle (2.8 eV/Ti) is 0.6 eV/Ti stronger than between Ti and C_{60} (2.2 eV) [210]. It is obvious that the clustering effect significantly reduces the gravimetric hydrogen storage capacity.

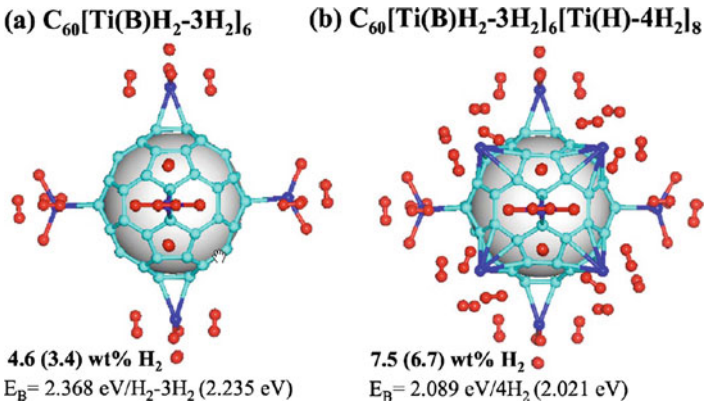

Fig. 15 Ti-coated C_{60} systems with high-density H coverage. Reprinted with permission from [210]. Copyright 2005, American Physical Society

Further, Sun et al. proposed lighter metals, such as alkali and alkali earth metals, coating C_{60} fullerenes to enhance hydrogen capacity [8, 212]. $Li_{12}C_{60}$ was found to have high gravimetric (9 wt%) and volumetric densities (70 g/L) [8]. Although Li metal tends to uniformly coat on the surface of C_{60}, the binding energies between $Li_{12}C_{60}$ and hydrogen molecules are very weak, with a maximum value of 0.075 eV. On the other hand, the weak binding energy (averaging 1.78 eV/Li) between Li and C_{60} may lead to instability of the structure at ambient temperature. Very recently, they also investigated Ca-coated C_{60} as hydrogen storage materials [212]. Ca tends to coat on the surface of C_{60} as single atoms rather than forming clusters. The calculated average binding energy increased to 0.45 eV/H_2 and the gravimetric density of this material can reach 6.2 wt%.

In fact, hydrogen storage capacity also can be increased by applying lighter-weight organic molecules or nanostructures, for example, boron nitride and boron fullerenes, as the supporter of metals [176, 213–215]. Li et al. studied Ca-coated boron fullerenes and nanotubes as hydrogen storage materials. They found that the B_{80} fullerene with 12 Ca can attract up to 60 H_2 molecules with binding energy 0.12–0.40 eV/H_2, corresponding to a 8.2 wt% capacity [216]. In addition, one must consider how many hydrogen molecules can be attracted by one metal atom. Very recently, Gagliardi and Pyykkö suggested the maximum number of 12 hydrogen atoms can be bound to one metal atom (Cr, Mo, W, V, and Ti) [217]. Therefore, the selectivity of a suitable metal plays an important role in increasing hydrogen storage capacity.

In addition, understanding the fundamental role of the carbon fullerene in hydrogen storage, as a support for metal or attractive sites for hydrogen molecules, is very important to improve hydrogen content. Yoon et al. studied charged fullerenes as hydrogen storage materials [218]. They found that the binding strength

of molecular hydrogen on either positively or negatively charged fullerenes can be dramatically enhanced to 0.18–0.32 eV, which ensures hydrogen storage at ambient conditions. At full hydrogen coverage, a charged fullerene can achieve storage capacities of more than ~8.0 wt%. The enhanced binding between charged fullerenes and hydrogen is attributed to the polarization of hydrogen molecules by the high electronic field generated near the surface of the charged fullerene. It suggests that both charged carbon fullerene and metals can be hosts for hydrogen molecules.

The hydrogen storage capacity in novel organometallic fullerenes and nanotubes is dependent on metal nanosize and structural properties of nanoparticles. The binding energy between hydrogen molecules and host plays an important role in validating hydrogen storage materials. Therefore, it is worth further discussing the interaction nature of host and hydrogen molecules. Niu et al. studied the binding of transition metal Ni and its ion with hydrogen molecules [177]. They found that only one hydrogen molecule can chemisorb dissociatively with a neutral Ni atom, forming a linear structure. The interaction between the Ni and hydrogen molecule is attributed to a consequence of the Pauli Exclusion Principle. In contrast, Ni^+ can bind several hydrogen molecules by electrostatic interaction. However, very recent computational studies showed that transition metals (Cr, Mo, W, Ti, and V) can not only break up the hydrogen molecule and form metal hydrides, but also that several hydrogen molecules can be adsorbed on the metal atom. The computational results showed that the more hydrogen molecules are adsorbed, the more stable metal hydrides became.

The interaction with hydrogen is enhanced due to the presence of metal, attributed to interaction between the charged metal and the induced dipole of the hydrogen molecule. However, this type of interaction is still not strong enough to allow hydrogen storage at ambient temperature. The molecular orbital analysis showed that there is a large hybridization among Ti-d, H-σ*, and C-p orbitals, as shown in Fig. 16 [209]. The mechanism of the bonding can be explained by the DCD donation-backdonation model. According to this model, electrons of Ti-d orbital are simultaneously donated to the π* antibonding orbital of C6 ring of SWNTN and σ* antibonding orbital of H–H. This weakens the H–H bond or causes H–H bond to break. Therefore, a combination of forces, including electron transfer and electrostatic interaction contribute to the overall effect. For transition metals, electron transfer interaction actually is the dominant force between H_2 and TM. In fact, electron transfer interaction is weakened because electrons in metals transferred to the low-energy π* in carbon system. With more hydrogen molecules being attracted to the TM site, electrostatic interaction will become more important. As a result, hydrogen adsorption takes the form of a hydrogen molecule after electrostatic interaction becomes dominant.

In summary, preventing the clustering of the coated metals and enhancing electrostatic interactions between the metals and hydrogen play an important role in designing novel hydrogen storage materials based on metal-coated SWNT and fullerenes.

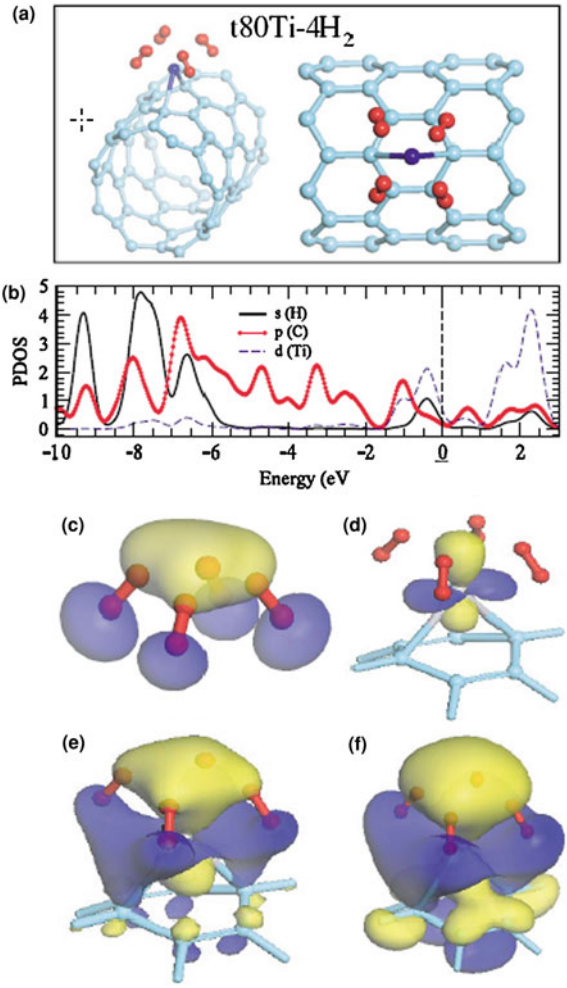

Fig. 16 Geometrical and electronic structures of Ti-coated carbon nanotube. **a** Two different views of the optimized structure of t80Ti-$4H_2$, **b** PDOS of Ti, C, and H atoms, **c** The σ^* antibonding orbital of four H_2 complex, **d–f** isosurface of the state just below E_f at three different values (0.08, 0.04, and 0.2). Reprinted with permission from [209]. Copyright 2005, American Physical Society

5 Concluding Remarks

Hydrogen storage has been a remarkably active field for research and development over the past decade. Nanoscience and nanotechnology have made a significant impact on hydrogen storage research. The new characterization techniques have started to provide unprecedented details of the system, including atomic and electronic structures. The new synthesis methods developed over the same period provide new opportunities to control the size, shape, and local composition on the nanometer scale. Developments in density functional theory-based computational methods led to a remarkable degree of reliability in structural analyses for systems relevant to hydrogen storage. Theoretical studies help to screen materials that are potentially useful for hydrogen storage. Theory also helps to search for and design

systems to have favorable properties for hydrogen storage. Nanosize effects have been studied both theoretically and experimentally. In this aspect, theoretical studies clearly demonstrated the improvement in both thermodynamic and kinetics for hydrogen storage. The structural and electronic analysis of the transition metal-doped hydride helps us understand the change in the hydrogen interaction induced by the transition metal and to select more effective catalysts and design new catalytic structures. Theoretical studies allow us to explore novel structures that have not yet been synthesized and predict their properties. The novel structures may be synthesized with the aid of the newly developed nanofabrication technology. We hope that the issues preventing hydrogen storage from becoming a reality will be overcome with the use of nanotechnology, as predicted by Professor Smalley, so that the hydrogen economy becomes a reality.

Acknowledgments We acknowledge support by U. S. Department of Energy, Basic Energy Science grant DE-FG02-05ER46231.

References

1. Baxter J, Bian ZX, Chen G, Danielson D, Dresselhaus MS, Fedorov AG, Fisher TS, Jones CW, Maginn E, Kortshagen U, Manthiram A, Nozik A, Rolison DR, Sands T, Shi L, Sholl D, Wu YY (2009) Nanoscale design to enable the revolution in renewable energy. Energy Environ Sci 2:559–588
2. Schlapbach L, Züttel A (2001) Hydrogen-storage materials for mobile applications. Nature 414:353–358
3. Crabtree GW, Dresselhaus MS, Buchanan MV (2004) The hydrogen economy. Phys Today 57(12):39–44
4. US DOE (2010) Hydrogen Storage http://hydrogenenergygov/storagehtml
5. von Helmolt R, Eberle U (2007) Fuel cell vehicles: status 2007. J Power Sour 165:833–843
6. Zaluska A, Zaluski L, Ström-Olsen JO (2001) Structure, catalysis and atomic reactions on the nano-scale: a systematic approach to metal hydrides for hydrogen storage. Appl Phys A: Mater Sci Process 72:157–165
7. Li YW, Yang RT (2006) Significantly enhanced hydrogen storage in metal-organic frameworks via spillover. J Am Chem Soc 128:726–727
8. Sun Q, Jena P, Wang Q, Marquez M (2006) First-principles study of hydrogen storage on $Li_{12}C_{60}$. J Am Chem Soc 128:9741–9745
9. Rosi NL, Eckert J, Eddaoudi M, Vodak DT, Kim J, O'Keeffe M, Yaghi OM (2003) Hydrogen storage in microporous metal-organic frameworks. Science 300:1127–1129
10. Han SS, Furukawa H, Yaghi OM, Goddard WA (2008) Covalent organic frameworks as exceptional hydrogen storage materials. J Am Chem Soc 130:11580
11. Hohenberg P, Kohn W (1964) Inhomogeneous electron gas. Phys Rev 136:B864
12. Kohn W, Sham LJ (1965) Self-consistent equations including exchange and correlation effects. Phys Rev 140:A1133
13. Graetz J (2009) New approaches to hydrogen storage. Chem Soc Rev 38:73–82
14. Wang LF, Yang RT (2008) New sorbents for hydrogen storage by hydrogen spillover - a review. Energy Environ Sci 1:268–279
15. Orimo SI, Nakamori Y, Eliseo JR, Züttel A, Jensen CM (2007) Complex hydrides for hydrogen storage. Chem Rev 107:4111–4132

16. van den Berg AWC and Arean CO (2008) Materials for hydrogen storage: current research trends and perspectives. Chem Commun. 668−681
17. Yang J, Sudik A, Wolverton C, Siegel DJ (2010) High capacity hydrogen storage materials: attributes for automotive applications and techniques for materials discovery. Chem Soc Rev 39:656–675
18. Finholt AE, Bond AC, Schlesinger HI (1947) Lithium aluminum hydride, aluminum hydride and lithium gallium hydride, and some of their applications in organic and inorganic chemistry. J Am Chem Soc 69:1199–1203
19. Bogdanović B, Schwickardi M (1997) Ti-doped alkali metal aluminium hydrides as potential novel reversible hydrogen storage materials. J Alloys Compd 253:1–9
20. Bogdanović B, Brand RA, Marjanović A, Schwickardi M, Tölle J (2000) Metal-doped sodium aluminium hydrides as potential new hydrogen storage materials. J Alloys Compd 302:36–58
21. Baroni S, de Gironcoli S, Dal Corso A, Giannozzi P (2001) Phonons and related crystal properties from density-functional perturbation theory. Rev Mod Phys 73:515–562
22. Vegge T (2006) Equilibrium structure and Ti-catalyzed H_2 desorption in $NaAlH_4$ nanoparticles from density functional theory. Phys Chem Chem Phys 8:4853–4861
23. Johnson CA, Chakerian GD (1965) On the proof and uniqueness of Wulff's construction of the shape of minimum surface free energy. J Math Phys 6:1403–1404
24. Kim KC, Dai B, Johnson JK, Sholl DS (2009) Assessing nanoparticle size effects on metal hydride thermodynamics using the Wulff construction. Nanotechnology 20:204001
25. Alapati SV, Johnson JK, Sholl DS (2007) Using first principles calculations to identify new destabilized metal hydride reactions for reversible hydrogen storage. Phys Chem Chem Phys 9:1438–1452
26. Løvvik OM, Swang O, Opalka SM (2005) Modeling alkali alanates for hydrogen storage by density-functional band-structure calculations. J Mater Res 20:3199–3213
27. Opalka SM, Løvvik OM, Brinks HW, Saxe PW, Hauback BC (2007) Integrated experimental-theoretical investigation of the Na-Li-Al-H system. Inorg Chem 46: 1401–1409
28. Huot J, Boily S, Güther V, Schulz R (1999) Synthesis of Na_3AlH_6 and Na_2LiAlH_6 by mechanical alloying. J Alloys Compd 283:304–306
29. Brinks HW, Hauback BC, Jensen CM, Zidan R (2005) Synthesis and crystal structure of Na_2LiAlD_6. J Alloys Compd 392:27–30
30. Tang X, Opalka SM, Laube BL, Wu FJ, Strickler JR, Anton DL (2007) Hydrogen storage properties of Na-Li-Mg-Al-H complex hydrides. J Alloys Compd 446:228–231
31. Grove H, Brinks HW, Heyn RH, Wu FJ, Opalka SM, Tang X, Laube BL, Hauback BC (2008) The structure of $LiMg(AlD_4)_3$. J Alloys Compd 455:249–254
32. Yamauchi M, Kobayashi H, Kitagawa H (2009) Hydrogen storage mediated by Pd and Pt nanoparticles. ChemPhysChem 10:2566–2576
33. Pundt A (2004) Hydrogen in nano-sized metals. Adv Eng Mater 6:11–21
34. Pundt A, Kirchheim R (2006) Hydrogen in metals: microstructural aspects. Ann Rev Mater Res 36:555–608
35. Baldé CP, Hereijgers BPC, Bitter JH, de Jong KP (2006) Facilitated hydrogen storage in $NaAlH_4$ supported on carbon nanoribers. Angew Chem-Int Edit 45:3501–3503
36. Baldé CP, Hereijgers BPC, Bitter JH, de Jong KP (2008) Sodium alanate nanoparticles - Linking size to hydrogen storage properties. J Am Chem Soc 130:6761–6765
37. Verkuijlen MHW, Gao J, Adelhelm P, van Bentum PJM, de Jongh PE, Kentgens APM (2010) Solid-state NMR studies of the local structure of $NaAlH_4$/C nanocomposites at different stages of hydrogen desorption and rehydrogenation. J Phys Chem C 114: 4683–4692
38. Gao J, Adelhelm P, Verkuijlen MHW, Rongeat C, Herrich M, van Bentum PJM, Gutfleisch O, Kentgens APM, de Jong KP, de Jongh PE (2010) Confinement of $NaAlH_4$ in nanoporous carbon: impact on H_2 release, reversibility, and thermodynamics. J Phys Chem C 114: 4675–4682

39. Balema VP, Balema L (2005) Missing pieces of the puzzle or about some unresolved issues in solid state chemistry of alkali metal aluminohydrides. Phys Chem Chem Phys 7: 1310–1314
40. Zheng SY, Fang F, Zhou GY, Chen GR, Ouyang LZ, Zhu M, Sun DL (2008) Hydrogen storage properties of space-confined $NaAlH_4$ nanoparticles in ordered mesoporous silica. Chem Mat 20:3954–3958
41. Bhakta RK, Herberg JL, Jacobs B, Highley A, Behrens R, Ockwig NW, Greathouse JA, Allendorf MD (2009) Metal-organic frameworks as templates for nanoscale $NaAlH_4$. J Am Chem Soc 131:13198
42. Züttel A, Rentsch S, Fischer P, Wenger P, Sudan P, Mauron P, Emmenegger C (2003) Hydrogen storage properties of $LiBH_4$. J Alloys Compd 356:515–520
43. Züttel A, Wenger P, Rentsch S, Sudan P, Mauron P, Emmenegger C (2003) $LiBH_4$ a new hydrogen storage material. J Power Sour 118:1–7
44. Lodziana Z, Vegge T (2004) Structural stability of complex hydrides: $LiBH_4$ revisited. Phys Rev Lett 93:145501
45. Orima S, Nakamori Y, Kitahara G, Miwa K, Ohba N, Towata S, Züttel A (2005) Dehydriding and rehydriding reactions of $LiBH_4$. J Alloys Compd 404:427–430
46. Ge Q (2004) Structure and energetics of $LiBH_4$ and its surfaces: a first-principles study. J Phys Chem A 108:8682–8690
47. Liu J, Ge Q (2009) Hydrogen interaction in Ti-doped $LiBH_4$ for hydrogen storage: a density functional analysis. J Chem Theory Comput 5:3079–3087
48. Kang XD, Wang P, Ma LP, Cheng HM (2007) Reversible hydrogen storage in $LiBH_4$ destabilized by milling with Al. Appl Phys A 89:963–966
49. Kostka J, Lohstroh W, Fichtner M, Hahn H (2007) Diborane release from $LiBH_4$/Silica-Gel mixtures and the effect of additives. J Phys Chem C 111:14026–14029
50. Nickels EA, Jones Martin O, David William IF, Johnson Simon R, Lowton Rebecca L, Sommariva M, Edwards Peter P (2008) Tuning the decomposition temperature in complex hydrides: synthesis of a mixed alkali metal Borohydride13. Angew Chem-Int Edit 47: 2817–2819
51. Claudy P, Bonnetot B, Letoffe JM, Turck G (1978) Determination des constantes thermodynamiques des hydrures simples et complexes de l'aluminium. IV. Enthalpie de formation de $LiAlH_2$ et Li_3AlH_6. Thermochimica Acta 27:213–221
52. Dymova TN, Aleksandrov DP, Konoplev VN, Silina TA, Sizareva AS (1994) Spontaneous and thermal-decomposition of Lithium Tetrahydroaluminate $LiAlH_4$ - the promoting effect of mechanochemical action on the process. Koord Khimiya 20:279–285
53. Balema VP, Dennis KW and Pecharsky VK (2000) Rapid solid-state transformation of tetrahedral AlH_4 (-) into octahedral AlH_6 (3-) in lithium aluminohydride. Chem Commun. 1665–1666
54. Balema VP, Pecharsky VK, Dennis KW (2000) Solid state phase transformations in $LiAlH_4$ during high-energy ball-milling. J Alloys Compd 313:69–74
55. Balema VP, Wiench JW, Dennis KW, Pruski M, Pecharsky VK (2001) Titanium catalyzed solid-state transformations in $LiAlH_4$ during high-energy ball-milling. J Alloys Compd 329:108–114
56. Chen J, Kuriyama N, Xu Q, Takeshita HT, Sakai T (2001) Reversible hydroen storage via titanium-catalyzed $LiAlH_4$ and Li_3AlH_6. J Phys Chem B 105:11214–11220
57. Alapati SV, Johnson JK, Sholl DS (2006) Identification of destabilized metal hydrides for hydrogen storage using first principles calculations. J Phys Chem B 110:8769–8776
58. Alapati SV, Johnson JK, Sholl DS (2007) Predicting reaction equilibria for destabilized metal hydride decomposition reactions for reversible hydrogen storage. J Phys Chem C 111:1584–1591
59. Yu XB, Grant DM and Walker GS (2006) A new dehydrogenation mechanism for reversible multicomponent borohydride systems - The role of Li-Mg alloys. Chem Commun. 3906–3908

60. Wolverton C, Siegel DJ, Akbarzadeh AR, Ozoliņš V (2008) Discovery of novel hydrogen storage materials: an atomic scale computational approach. J Phys-Condes Matter 20:14
61. Siegel DJ, Wolverton C, Ozoliņš V (2007) Thermodynamic guidelines for the prediction of hydrogen storage reactions and their application to destabilized hydride mixtures. Phys Rev B 76:134102
62. Vajo JJ, Olson GL (2007) Hydrogen storage in destabilized chemical systems. Scr Mater 56:829–834
63. Fang ZZ, Kang XD, Dai HB, Zhang MJ, Wang P, Cheng HM (2008) Reversible dehydrogenation of $LiBH_4$ catalyzed by as-prepared single-walled carbon nanotubes. Scr Mater 58:922–925
64. Vajo JJ, Skeith SL, Mertens F (2005) Reversible storage of hydrogen in destabilized $LiBH_4$. J Phys Chem B 109:3719–3722
65. Yu XB, Grant DM, Walker GS (2009) Dehydrogenation of $LiBH_4$ destabilized with various oxides. J Phys Chem C 113:17945–17949
66. Au M, Jurgensen A, Zeigler K (2006) Modified lithium borohydrides for reversible hydrogen storage (2). J Phys Chem B 110:26482–26487
67. Zhang Y, Zhang WS, Wang AQ, Sun LX, Fan MQ, Chu HL, Sun JC, Zhang T (2007) $LiBH_4$ nanoparticles supported by disordered mesoporous carbon: hydrogen storage performances and destabilization mechanisms. Int J Hydrogen Energy 32:3976–3980
68. Au M, Jurgensen AR, Spencer WA, Anton DL, Pinkerton FE, Hwang SJ, Kim C, Bowman RC (2008) Stability and reversibility of lithium borohydrides doped by metal halides and hydrides. J Phys Chem C 112:18661–18671
69. Gross AF, Vajo JJ, Van Atta SL, Olson GL (2008) Enhanced hydrogen storage kinetics of $LiBH_4$ in nanoporous carbon scaffolds. J Phys Chem C 112:5651–5657
70. Walker GS, Grant DM, Price TC, Yu XB, Legrand V (2009) High capacity multicomponent hydrogen storage materials: investigation of the effect of stoichiometry and decomposition conditions on the cycling behaviour of $LiBH_4$-MgH_2. J Power Sources 194:1128–1134
71. Opalka SM, Tang X, Laube BL, Vanderspurt TH (2009) Experimental and theoretical screening of nanoscale oxide reactivity with $LiBH_4$. Nanotechnology 20:204024
72. Oguchi H, Matsuo M, Hummelshoj JS, Vegge T, Norskov JK, Sato T, Miura Y, Takamura H, Maekawa H, Orimo S (2009) Experimental and computational studies on structural transitions in the $LiBH_4$-LiI pseudobinary system. Appl Phys Lett 94:141912
73. Somorjai GA, Borodko YG (2001) Research in Nanosciences–Great opportunity for Catalysis Science. Catal Lett 76:1–5
74. Berseth PA, Harter AG, Zidan R, Blomqvist A, Araújo CM, Scheicher RH, Ahuja R, Jena P (2009) Carbon nanomaterials as catalysts for hydrogen uptake and release in $NaAlH_4$. Nano Lett 9:1501–1505
75. Singh S, Eijt SWH, Huot J, Kockelmann WA, Wagernaker M, Mulder FM (2007) The $TiCl_3$ catalyst in $NaAlH_4$ for hydrogen storage induces grain refinement and impacts on hydrogen vacancy formation. Acta Mater 55:5549–5557
76. Lee GJ, Shim JH, Cho YW, Lee KS (2007) Reversible hydrogen storage in $NaAlH_4$ catalyzed with lanthanide oxides. Int J Hydrogen Energy 32:1911–1915
77. Felderhoff M, Weidenthaler C, von Helmolt R, Eberle U (2007) Hydrogen storage: the remaining scientific and technological challenges. Phys Chem Chem Phys 9:2643–2653
78. Baldé CP, Stil HA, van der Eerden AMJ, de Jong KP, Bitter JH (2007) Active Ti species in $TiCl_3$-doped $NaAlH_4$. mechanism for catalyst deactivation. J Phys Chem C 111:2797–2802
79. Léon A, Schild D, Fichtner M (2006) Chemical state of Ti in sodium alanate doped with $TiCl_3$ using X-ray photoelectron spectroscopy (vol 404, pg 766, 2005). J Alloys Compd 407:340–340
80. Léon A, Kircher O, Rösner H, Décamps B, Leroy E, Fichtner M, Percheron-Guégan A (2006) SEM and TEM characterization of sodium alanate doped with $TiCl_3$ or small Ti clusters (Ti_{13} * 6THF). J Alloys Compd 414:190–203

81. Léon A, Kircher O, Fichtner M, Rothe J, Schild D (2006) Evolution of the local structure around Ti atoms in $NaAlH_4$ doped with $TiCl_3$ or Ti_{13} center dot 6THF by ball milling using X-ray absorption and X-ray photoelectron spectroscopy. J Phys Chem B 110:1192–1200
82. Canton P, Fichtner M, Frommen C, Léon A (2006) Synchrotron X-ray studies of Ti-doped $NaAlH_4$. J Phys Chem B 110:3051–3054
83. Brinks HW, Sulic M, Jensen CM, Hauback BC (2006) $TiCl_3$-enhanced $NaAlH_4$: impact of excess Al and development of the Al1-gamma Ti gamma phase during cycling. J Phys Chem B 110:2740–2745
84. Bogdanović B, Felderhoff M, Pommerin A, Schüth T, Spielkamp N (2006) Advanced hydrogen-storage materials based on Sc-, Ce-, and Pr-doped $NaAlH_4$. Adv Mater 18:1198
85. Bellosta von Colbe JM, Schmidt W, Felderhoff M, Bogdanović B, Schüth F (2006) Hydrogen-isotope scrambling on doped sodium alanate. Angew Chem-Int Edit 45: 3663–3665
86. Wang P, Kang XD, Cheng HM (2005) Exploration of the nature of active Ti species in metallic Ti-doped $NaAlH_4$. J Phys Chem B 109:20131–20136
87. Wang J, Ebner AD, Zidan R, Ritter JA (2005) Synergistic effects of co-dopants on the dehydrogenation kinetics of sodium aluminum hydride. J Alloys Compd 391:245–255
88. von Colbe JMB, Felderhoff M, Bogdanović B, Schüth F and Weidenthaler C (2005) One-step direct synthesis of a Ti-doped sodium alanate hydrogen storage material. Chem Commun. 4732–4734
89. Resan M, Hampton MD, Lomness JK, Slattery DK (2005) Effect of TixAly catalysts on hydrogen storage properties of $LiAlH_4$ and $NaAlH_4$. Int J Hydrogen Energy 30:1417–1421
90. Majer G, Stanik E, Banuet LEV, Grinberg F, Kircher O, Fichtner M (2005) Effects of catalysts on the dehydriding of alanates monitored by proton NMR. J Alloys Compd 404:738–742
91. Léon A, Schild D, Fichtner M (2005) Chemical state of Ti in sodium alanate doped with $TiCl_3$ using X-ray photoelectron spectroscopy. J Alloys Compd 404:766–770
92. Isobe S, Ichikawa T, Hanada N, Leng HY, Fichtner M, Fuhr O, Fujii H (2005) Effect of Ti catalyst with different chemical form on Li-N-H hydrogen storage properties. J Alloys Compd 404:439–442
93. Gomes S, Renaudin G, Hagemann H, Yvon K, Sulic MP, Jensen CM (2005) Effects of milling, doping and cycling of $NaAlH_4$ studied by vibrational spectroscopy and X-ray diffraction. J Alloys Compd 390:305–313
94. Haiduc AG, Stil HA, Schwarz MA, Paulus P, Geerlings JJC (2005) On the fate of the Ti catalyst during hydrogen cycling of sodium alanate. J Alloys Compd 393:252–263
95. Bellosta von Colbe JM, Felderhoff M, Bogdanović B, Schüth F and Weidenthaler C (2005) One-step direct synthesis of a Ti-doped sodium alanate hydrogen storage material. Chem Commun: 4732–4734
96. Wang P, Jensen CM (2004) Preparation of Ti-doped sodium aluminum hydride from mechanical milling of NaH/Al with off-the-shelf Ti powder. J Phys Chem B 108: 15827–15829
97. Wang P, Jensen CM (2004) Method for preparing Ti-doped $NaAlH_4$ using Ti powder: observation of an unusual reversible dehydrogenation behavior. J Alloys Compd 379: 99–102
98. Srinivasan SS, Brinks HW, Hauback BC, Sun DL, Jensen CM (2004) Long term cycling behavior of titanium doped $NaAlH_4$ prepared through solvent mediated milling of NaH and Al with titanium dopant precursors. J Alloys Compd 377:283–289
99. Bogdanović B, Felderhoff M, Kaskel S, Pommerin A, Schlichte K, Schüth F (2003) Improved hydrogen storage properties of Ti-doped sodium alanate using titanium nanoparticles as doping agents. Adv Mater 15:1012
100. Bogdanović B, Felderhoff M, Germann M, Hartel M, Pommerin A, Schüth F, Weidenthaler C, Zibrowius B (2003) Investigation of hydrogen discharging and recharging processes of Ti-doped $NaAlH_4$ by X-ray diffraction analysis (XRD) and solid-state NMR spectroscopy. J Alloys Compd 350:246–255

101. Thomas GJ, Gross KJ, Yang NYC, Jensen C (2002) Microstructural characterization of catalyzed $NaAlH_4$. J Alloys Compd 330:702–707
102. Sandrock G, Gross K, Thomas G (2002) Effect of Ti-catalyst content on the reversible hydrogen storage properties of the sodium alanates. J Alloys Compd 339:299–308
103. Bogdanović B, Schwickardi M (2001) Ti-doped $NaAlH_4$ as a hydrogen-storage material - preparation by Ti-catalyzed hydrogenation of aluminum powder in conjunction with sodium hydride. Appl Phys A 72:221–223
104. Zaluska A, Zaluski L, Ström-Olsen JO (2000) Sodium alanates for reversible hydrogen storage. J Alloys Compd 298:125–134
105. Zidan RA, Takara S, Hee AG, Jensen CM (1999) Hydrogen cycling behavior of zirconium and titanium-zirconium-doped sodium aluminum hydride. J Alloys Compd 285:119–122
106. Jensen CM, Zidan R, Mariels N, Hee A, Hagen C (1999) Advanced titanium doping of sodium aluminum hydride: segue to a practical hydrogen storage material? Int J Hydrogen Energy 24:461–465
107. Stephens RD, Gross AF, Van Atta SL, Vajo JJ, Pinkerton FE (2009) The kinetic enhancement of hydrogen cycling in $NaAlH_4$ by melt infusion into nanoporous carbon aerogel. Nanotechnology 20:204018
108. Adelhelm P, de Jong KP and de Jongh PE (2009) How intimate contact with nanoporous carbon benefits the reversible hydrogen desorption from NaH and $NaAlH_4$. Chem Commun. 6261–6263
109. Shi Q, Yu X, Feidenhans'l R, Vegge T (2008) Destabilized $LiBH_4$-$NaAlH_4$ Mixtures Doped with Titanium Based Catalysts. J Phys Chem C 112:18244–18248
110. Majzoub EH, Ozolinš V (2008) Prototype electrostatic ground state approach to predicting crystal structures of ionic compounds: application to hydrogen storage materials. Phys Rev B 77:104115
111. Yin LC, Wang P, Kang XD, Sun CH, Cheng HM (2007) Functional anion concept: effect of fluorine anion on hydrogen storage of sodium alanate. Phys Chem Chem Phys 9:1499–1502
112. Wang J, Ebner AD, Ritter JA (2007) Synthesis of metal complex hydrides for hydrogen storage. J Phys Chem C 111:14917–14924
113. Graetz J, Reilly JJ, Johnson J, Ignatov AY, Tyson TA (2004) X-ray absorption study of Ti-activated sodium aluminum hydride. Appl Phys Lett 85:500–502
114. Schüth F, Bogdanović B, Felderhoff M (2004) Light metal hydrides and complex hydrides for hydrogen storage. Chem Commun: 2249–2258
115. Felderhoff M, Klementiev K, Grunert W, Spliethoff B, Tesche B, Bellosta von Colbe JM, Bogdanović B, Hartel M, Pommerin A, Schüth F, Weidenthaler C (2004) Combined TEM-EDX and XAFS studies of Ti-doped sodium alanate. Phys Chem Chem Phys 6:4369–4374
116. Kang XD, Wang P, Song XP, Yao XD, Lu GQ, Cheng HM (2006) Catalytic effect of Al_3Ti on the reversible dehydrogenation of $NaAlH_4$. J Alloys Compd 424:365–369
117. Weidenthaler C, Pommerin A, Felderhoff M, Bogdanović B, Schüth F (2003) On the state of the titanium and zirconium in Ti- or Zr-doped $NaAlH_4$ hydrogen storage material. Phys Chem Chem Phys 5:5149–5153
118. Gross KJ, Majzoub EH, Spangler SW (2003) The effects of titanium precursors on hydriding properties of alanates. J Alloys Compd 356:423–428
119. Gross KJ, Guthrie S, Takara S, Thomas G (2000) In situ X-ray diffraction study of the decomposition of $NaAlH_4$. J Alloys Compd 297:270–281
120. Gross KJ, Sandrock G, Thomas GJ (2002) Dynamic in situ X-ray diffraction of catalyzed alanates. J Alloys Compd 330:691–695
121. Voss J, Shi Q, Jacobsen HS, Zamponi M, Lefmann K, Vegge T (2007) Hydrogen dynamics in Na_3AlH_6: a combined density functional theory and quasielastic neutron scattering study. J Phys Chem B 111:3886–3892
122. Løvvik OM, Opalka SM (2006) Stability of Ti in $NaAlH_4$. Appl Phys Lett 88:161917
123. Løvvik OM, Opalka SA (2005) Density functional calculations of Ti-enhanced $NaAlH_4$. Phys Rev B 71:054103

124. Íñiguez J, Yildirim T, Udovic TJ, Sulic M, Jensen CM (2004) Structure and hydrogen dynamics of pure and Ti-doped sodium alanate. Phys Rev B 70:060101
125. Íñiguez J, Yildirim T (2005) First-principles study of Ti-doped sodium alanate surfaces. Appl Phys Lett 86:103109
126. Araújo CM, Li S, Ahuja R, Jena P (2005) Vacancy-mediated hydrogen desorption in $NaAlH_4$. Phys Rev B 72:165101
127. Du AJ, Smith SC, Lu GQ (2007) Vacancy mediated desorption of hydrogen from a sodium alanate surface: an ab initio spin-polarized study. Appl Phys Lett 90:143119
128. Liu J and Ge Q (2006) A precursor state for formation of $TiAl_3$ complex in reversible hydrogen desorption/adsorption from Ti-doped $NaAlH_4$. Chem Commun. 1822–1824
129. Liu J, Ge Q (2006) A first-principles analysis of hydrogen interaction in Ti-doped $NaAlH_4$ surfaces: structure and energetics. J Phys Chem B 110:25863–25868
130. Liu J, Ge Q (2007) A first-principles study of Sc-doped $NaAlH_4$ for reversible hydrogen storage. J Alloys Compd 446–447:267–270
131. Liu J, Han Y, Ge Q (2009) Effect of doped transition metal on reversible hydrogen release/uptake from $NaAlH_4$. Chem Eur J 15:1685–1695
132. Kubas GJ (2009) Hydrogen activation on organometallic complexes and H_2 production, utilization, and storage for future energy. J Organomet Chem 694:2648–2653
133. Chaudhuri S, Rangan S, Veyan JF, Muckerman JT, Chabal YJ (2008) Formation and bonding of alane clusters on Al(111) surfaces studied by infrared absorption spectroscopy and theoretical modeling. J Am Chem Soc 130:10576–10587
134. Chaudhuri S, Muckerman JT (2005) First-principles study of Ti-catalyzed hydrogen chemisorption on an Al surface: a critical first step for reversible hydrogen storage in $NaAlH_4$. J Phys Chem B 109:6952–6957
135. Ljubić I, Clary DC (2010) Towards understanding a mechanism for reversible hydrogen storage: theoretical study of transition metal catalysed dehydrogenation of sodium alanate. Phys Chem Chem Phys 12:4012–4023
136. Anton DL (2003) Hydrogen desorption kinetics in transition metal modified $NaAlH_4$. J Alloys Compd 356:400–404
137. Au M, Jurgensen A (2006) Modified Lithium Borohydrides for Reversible Hydrogen Storage. J Phys Chem B 110:7062–7067
138. Gunaydin H, Houk KN, Ozoliņš V (2008) Vacancy-mediated dehydrogenation of sodium alanate. Proc Natl Acad Sci 105:3673–3677
139. Grochala W, Edwards PP (2004) Thermal decomposition of the non-interstitial hydrides for the storage and production of hydrogen. Chem Rev 104:1283–1315
140. Bogdanović B, Ritter A, Spliethoff B (1990) Active MgH_2-Mg systems for reversible cehmical energy storage. Angew Chem Int Edit 29:223–234
141. Du AJ, Smith SC, Yao XD, Lu GQ (2007) Hydrogen spillover mechanism on a Pd-doped Mg surface as revealed by ab initio density functional calculation. J Am Chem Soc 129:10201–10204
142. Yoshimura K, Yamada Y, Okada M (2004) Hydrogenation of Pd capped Mg thin films at room temperature. Surf Sci 566:751–754
143. Shalaan E, Schmitt H (2006) Mg nanoparticle switchable mirror films with improved absorption-desorption kinetics. Surf Sci 600:3650–3653
144. Berlouis LEA, Honnor P, Hall PJ, Morris S, Dodd SB (2006) An investigation of the effect of Ti, Pd and Zr on the dehydriding kinetics of MgH_2. J Mater Sci 41:6403–6408
145. Saita I, Li LQ, Saito K, Akiyama T (2003) Hydriding combustion synthesis of Mg_2NiH_4. J Alloys Compd 356:490–493
146. Aguey-Zinsou KF, Ares-Fernandez JR (2008) Synthesis of colloidal magnesium: a near room temperature store for hydrogen. Chem Mat 20:376–378
147. de Jongh PE, Wagemans RWP, Eggenhuisen TM, Dauvillier BS, Radstake PB, Meeldijk JD, Geus JW, de Jong KP (2007) The preparation of carbon-supported magnesium nanoparticles using melt infiltration. Chem Mat 19:6052–6057

148. Li WY, Li CS, Ma H, Chen J (2007) Magnesium nanowires: enhanced kinetics for hydrogen absorption and desorption. J Am Chem Soc 129:6710
149. Kooi BJ, Palasantzas G, De Hosson JTM (2006) Gas-phase synthesis of magnesium nanoparticles: a high-resolution transmission electron microscopy study. Appl Phys Lett 89:161914
150. Schimmel HG, Huot J, Chapon LC, Tichelaar FD, Mulder FM (2005) Hydrogen cycling of niobium and vanadium catalyzed nanostructured magnesium. J Am Chem Soc 127: 14348–14354
151. Bystrzycki J, Płociński T, Zieliński W, Wiśniewski Z, Polanski M, Mróz W, Bojar Z, Kurzdlowski KJ (2009) Nano-engineering of magnesium hydride for hydrogen storage. Microelectron Eng 86:889–891
152. Huot J, Tremblay ML, Schulz R (2003) Synthesis of nanocrystalline hydrogen storage materials. J Alloys Compd 356:603–607
153. de Castro JFR, Yavari AR, LeMoulec A, Ishikawa TT, Botta WJ (2005) Improving H-sorption in MgH_2 powders by addition of nanoparticles of transition metal fluoride catalysts and mechanical alloying. J Alloys Compd 389:270–274
154. Dehouche Z, Peretti HA, Hamoudi S, Yoo Y, Belkacemi K (2008) Effect of activated alloys on hydrogen discharge kinetics of MgH_2 nanocrystals. J Alloys Compd 455:432–439
155. Lu HB, Poh CK, Zhang LC, Guo ZP, Yu XB, Liu HK (2009) Dehydrogenation characteristics of Ti- and Ni/Ti-catalyzed Mg hydrides. J Alloys Compd 481:152–155
156. Tanaka K, Miwa T, Sasaki K, Kuroda K (2009) TEM studies of nanostructure in melt-spun Mg-Ni-La alloy manifesting enhanced hydrogen desorbing kinetics. J Alloys Compd 478:308–316
157. Wagemans RWP, van Lenthe JH, de Jongh PE, van Dillen AJ, de Jong KP (2005) Hydrogen storage in magnesium clusters: quantum chemical study. J Am Chem Soc 127:16675–16680
158. Cheung S, Deng WQ, van Duin ACT, Goddard WA (2005) ReaxFF(MgH) reactive force field for magnesium hydride systems. J Phys Chem A 109:851–859
159. Aguey-Zinsou KF, Fernandez JRA, Klassen T, Bormann R (2007) Effect of Nb_2O_5 on MgH_2 properties during mechanical milling. Int J Hydrogen Energy 32:2400–2407
160. Larsson P, Araújo CM, Larsson JA, Jena P, Ahuja R (2008) Role of catalysts in dehydrogenation of MgH_2 nanoclusters. Proc Natl Acad Sci 105:8227–8231
161. Hanada N, Ichikawa T, Isobe S, Nakagawa T, Tokoyoda K, Honma T, Fujii H, Kojima Y (2009) X-ray absorption spectroscopic study on valence state and local atomic structure of transition metal oxides doped in MgH_2. J Phys Chem C 113:13450–13455
162. Hanada N, Ichikawa T, Fujii H (2005) Catalytic effect of nanoparticle 3D-transition metals on hydrogen storage properties in magnesium hydride MgH_2 prepared by mechanical milling. J Phys Chem B 109:7188–7194
163. Hanada N, Ichikawa I, Fujii H (2005) Catalytic effect of Ni nano-particle and Nb oxide on H-desorption properties in MgH_2 prepared by ball milling. J Alloys Compd 404:716–719
164. Dillon AC, Jones KM, Bekkedahl TA, Kiang CH, Bethune DS, Heben MJ (1997) Storage of hydrogen in single-walled carbon nanotubes. Nature 386:377–379
165. Cheng HS, Chen L, Cooper AC, Sha XW, Pez GP (2008) Hydrogen spillover in the context of hydrogen storage using solid-state materials. Energy Environ Sci 1:338–354
166. Züttel A, Orimo S (2002) Hydrogen in nanostructured, carbon-related, and metallic materials. MRS Bull 27:705–711
167. Wong-Foy AG, Matzger AJ, Yaghi OM (2006) Exceptional H_2 saturation uptake in microporous metal-organic frameworks. J Am Chem Soc 128:3494–3495
168. Zhao D, Yuan DQ, Zhou HC (2008) The current status of hydrogen storage in metal-organic frameworks. Energy Environ Sci 1:222–235
169. Li JR, Kuppler RJ, Zhou HC (2009) Selective gas adsorption and separation in metal-organic frameworks. Chem Soc Rev 38:1477–1504
170. Bhatia SK, Myers AL (2006) Optimum conditions for adsorptive storage. Langmuir 22: 1688–1700

171. Dinca M, Yu AF, Long JR (2006) Microporous metal-organic frameworks incorporating 1, 4-benzeneditetrazolate: syntheses, structures, and hydrogen storage properties. J Am Chem Soc 128:8904–8913
172. Dinca M, Dailly A, Liu Y, Brown CM, Neumann DA, Long JR (2006) Hydrogen storage in a microporous metal-organic framework with exposed Mn^{2+} coordination sites. J Am Chem Soc 128:16876–16883
173. Rowsell JLC, Millward AR, Park KS, Yaghi OM (2004) Hydrogen sorption in functionalized metal-organic frameworks. J Am Chem Soc 126:5666–5667
174. Rowsell JLC, Eckert J, Yaghi OM (2005) Characterization of H_2 binding sites in prototypical metal-organic frameworks by inelastic neutron scattering. J Am Chem Soc 127:14904–14910
175. Chatt J, Duncanson LA (1953) Olefin co-ordination compounds. Part III. Infra-red spectra and structure: attempted preparation of acetylene complexes. J Chem Soc 2939–2947
176. Zhao YF, Kim YH, Dillon AC, Heben MJ, Zhang SB (2005) Hydrogen storage in novel organometallic buckyballs. Phys Rev Lett 94:155504
177. Niu J, Rao BK and Jena P (1992) Binding of hydrogen molecules by a transition-metal ion. Phys Rev Lett 68:2277–2280
178. Belof JL, Stern AC, Eddaoudi M, Space B (2007) On the mechanism of hydrogen storage in a metal-organic framework material. J Am Chem Soc 129:15202–15210
179. Zhou W, Yildirim T (2008) Nature and tunability of enhanced hydrogen binding in metal-organic frameworks with exposed transition metal sites. J Phys Chem C 112:8132–8135
180. Kaye SS, Dailly A, Yaghi OM, Long JR (2007) Impact of preparation and handling on the hydrogen storage properties of Zn_4O(1, 4-benzenedicarboxylate)(3) (MOF-5). J Am Chem Soc 129:14176
181. Chen BL, Ockwig NW, Millward AR, Contreras DS, Yaghi OM (2005) High H_2 adsorption in a microporous metal-organic framework with open metal sites. Angew Chem-Int Edit 44:4745–4749
182. Zhou W, Wu H, Yildirim T (2008) Enhanced H_2 adsorption in isostructural metal-organic frameworks with open metal sites: strong dependence of the binding strength on metal ions. J Am Chem Soc 130:15268
183. Sun YY, Kim YH, Zhang SB (2007) Effect of spin state on the dihydrogen binding strength to transition metal centers in metal-organic frameworks. J Am Chem Soc 129:12606
184. Frost H, Duren T, Snurr RQ (2006) Effects of surface area, free volume, and heat of adsorption on hydrogen uptake in metal-organic frameworks. J Phys Chem B 110: 9565–9570
185. Lochan RC, Head-Gordon M (2006) Computational studies of molecular hydrogen binding affinities: the role of dispersion forces, electrostatics, and orbital interactions. Phys Chem Chem Phys 8:1357–1370
186. Han SS, Deng WQ, Goddard WA (2007) Improved designs of metal-organic frameworks for hydrogen storage. Angew Chem-Int Edit 46:6289–6292
187. Frost H, Snurr RQ (2007) Design requirements for metal-organic frameworks as hydrogen storage materials. J Phys Chem C 111:18794–18803
188. Han SS, Goddard WA (2007) Lithium-doped metal-organic frameworks for reversible H_2 storage at ambient temperature. J Am Chem Soc 129:8422
189. Mulfort KL, Hupp JT (2007) Chemical reduction of metal-organic framework materials as a method to enhance gas uptake and binding. J Am Chem Soc 129:9604
190. Blomqvist A, Araújo CM, Srepusharawoot P, Ahuja R (2007) Li-decorated metal-organic framework 5: a route to achieving a suitable hydrogen storage medium. Proc Natl Acad Sci 104:20173–20176
191. Mavrandonakis A, Tylianakis E, Stubos AK, Froudakis GE (2008) Why Li doping in MOFs enhances H_2 storage capacity? A multi-scale theoretical study. J Phys Chem C 112: 7290–7294

192. Klontzas E, Mavrandonakis A, Tylianakis E, Froudakis GE (2008) Improving hydrogen storage capacity of MOF bv functionalization of the organic linker with lithium atoms. Nano Lett 8:1572–1576
193. Lan J, Cao D, Wang W (2010) Li-doped and nondoped covalent organic borosilicate framework for hydrogen storage. J Phys Chem C 114:3108–3114
194. Cao D, Lan J, Wang W, Smit B (2009) Lithium-doped 3D covalent organic frameworks: high-capacity hydrogen storage materials. Angew Chem Int Edit 48:4730–4733
195. Kesanli B, Cui Y, Smith MR, Bittner EW, Bockrath BC, Lin WB (2005) Highly interpenetrated metal-organic frameworks for hydrogen storage. Angew Chem-Int Edit 44:72–75
196. Rowsell JLC, Yaghi OM (2006) Effects of functionalization, catenation, and variation of the metal oxide and organic linking units on the low-pressure hydrogen adsorption properties of metal-organic frameworks. J Am Chem Soc 128:1304–1315
197. Orimo S, Züttel A, Schlapbach L, Majer G, Fukunaga T, Fujii H (2003) Hydrogen interaction with carbon nanostructures: current situation and future prospects. J Alloys Compd 356:716–719
198. Wu XB, Chen P, Lin J, Tan KL (2000) Hydrogen uptake by carbon nanotubes. Int J Hydrogen Energy 25:261–265
199. Chambers A, Park C, Baker RTK, Rodriguez NM (1998) Hydrogen storage in graphite nanofibers. J Phys Chem B 102:4253–4256
200. Ye Y, Ahn CC, Witham C, Fultz B, Liu J, Rinzler AG, Colbert D, Smith KA, Smalley RE (1999) Hydrogen adsorption and cohesive energy of single-walled carbon nanotubes. Appl Phys Lett 74:2307–2309
201. Darkrim FL, Malbrunot P, Tartaglia GP (2002) Review of hydrogen storage by adsorption in carbon nanotubes. Int J Hydrogen Energy 27:193–202
202. Shiraishi M, Takenobu T, Ata M (2003) Gas-solid interactions in the hydrogen/single-walled carbon nanotube system. Chem Phys Lett 367:633–636
203. Kajiura H, Tsutsui S, Kadono K, Kakuta M, Ata M, Murakami Y (2003) Hydrogen storage capacity of commercially available carbon materials at room temperature. Appl Phys Lett 82:1105–1107
204. Dag S, Ozturk Y, Ciraci S, Yildirim T (2005) Adsorption and dissociation of hydrogen molecules on bare and functionalized carbon nanotubes. Phys Rev B 72:155404
205. Kim BJ, Lee YS, Park SJ (2008) A study on the hydrogen storage capacity of Ni-plated porous carbon nanofibers. Int J Hydrogen Energy 33:4112–4115
206. Kim HS, Lee H, Han KS, Kim JH, Song MS, Park MS, Lee JY, Kang JK (2005) Hydrogen storage in Ni nanoparticle-dispersed multiwalled carbon nanotubes. J Phys Chem B 109:8983–8986
207. Liu C, Chen Y, Wu CZ, Xu ST, Cheng HM (2010) Hydrogen storage in carbon nanotubes revisited. Carbon 48:452–455
208. Jordá-Beneyto M, Suárez-García F, Lozano-Castelló D, Cazorla-Amorós D, Linares-Solano A (2007) Hydrogen storage on chemically activated carbons and carbon nanomaterials at high pressures. Carbon 45:293–303
209. Yildirim T, Ciraci S (2005) Titanium-decorated carbon nanotubes as a potential high-capacity hydrogen storage medium. Phys Rev Lett 94:175501
210. Yildirim T, Íñiguez J, Ciraci S (2005) Molecular and dissociative adsorption of multiple hydrogen molecules on transition metal decorated C_{60}. Phys Rev B 72:153403
211. Sun Q, Wang Q, Jena P, Kawazoe Y (2005) Clustering of Ti on a C_{60} surface and its effect on hydrogen storage. J Am Chem Soc 127:14582–14583
212. Wang Q, Sun Q, Jena P, Kawazoe Y (2009) Theoretical study of hydrogen storage in Ca-Coated fullerenes. J Chem Theory Comput 5:374–379
213. Kiran B, Kandalam AK, Jena P (2006) Hydrogen storage and the 18-electron rule. J Chem Phys 124:224703
214. Shevlin SA, Guo ZX (2006) Transition-metal-doping-enhanced hydrogen storage in boron nitride systems. Appl Phys Lett 89:153104

215. Shevlin SA, Guo ZX (2008) High-capacity room-temperature hydrogen storage in carbon nanotubes via defect-modulated Titanium doping. J Phys Chem C 112:17456–17464
216. Li M, Li Y, Zhou Z, Shen P, Chen Z (2009) Ca-Coated boron fullerenes and nanotubes as superior hydrogen storage materials. Nano Lett 9:1944–1948
217. Gagliardi L, Pyykkö P (2004) How many hydrogen atoms can be bound to a metal? Predicted MH_{12} species. J Am Chem Soc 126:15014–15015
218. Yoon M, Yang SY, Wang E, Zhang ZY (2007) Charged fullerenes as high-capacity hydrogen storage media. Nano Lett 7:2578–2583